ORIGINAL RESEARCH

A Systems Biology Approach to Investigating Sex Differences in Cardiac Hypertrophy

Josephine Harrington, MD;* Natasha Fillmore, PhD;* Shouguo Gao, PhD;* Yanqin Yang, MD;* Xue Zhang, PhD; Poching Liu, PhD; Andrea Stoehr, PhD; Ye Chen, PhD; Danielle Springer, VMD; Jun Zhu, PhD; Xujing Wang, PhD; Elizabeth Murphy, PhD

***Background*—**Heart failure preceded by hypertrophy is a leading cause of death, and sex differences in hypertrophy are well known, although the basis for these sex differences is poorly understood.

***Methods and Results*—**This study used a systems biology approach to investigate mechanisms underlying sex differences in cardiac hypertrophy. Male and female mice were treated for 2 and 3 weeks with angiotensin II to induce hypertrophy. Sex differences in cardiac hypertrophy were apparent after 3 weeks of treatment. RNA sequencing was performed on hearts, and sex differences in mRNA expression at baseline and following hypertrophy were observed, as well as within-sex differences between baseline and hypertrophy. Sex differences in mRNA were substantial at baseline and reduced somewhat with hypertrophy, as the mRNA differences induced by hypertrophy tended to overwhelm the sex differences. We performed an integrative analysis to identify mRNA networks that were differentially regulated in the 2 sexes by hypertrophy and obtained a network centered on PPARα (peroxisome proliferator-activated receptor α). Mouse experiments further showed that acute inhibition of PPARα blocked sex differences in the development of hypertrophy.

***Conclusions*—**The data in this study suggest that PPARα is involved in the sex-dimorphic regulation of cardiac hypertrophy. **(*J Am Heart Assoc*. 2017;6:e005838. DOI: 10.1161/JAHA.117.005838.)**

Key Words: hypertrophy • sex • systems biology

Heart failure (HF) is the leading cause of death in industrialized nations, and hypertrophy is a strong predictor of HF. Sex differences in hypertrophy have been observed; premenopausal women exhibit lower rates of cardiac hypertrophy than their male counterparts.[1,2] HF with preserved ejection fraction is also more common in women.[3–5] Studies in rodent models demonstrate that when exposed to a predisposing factor or stimulus, females develop less hypertrophy than their male cohorts, even when exposed to identical levels of pathologic insult such as angiotensin II or transaortic constriction.[6–10]

Despite evidence that sex-based differences exist between men and premenopausal women in HF and other forms of heart disease,[1] large randomized clinical trials have not demonstrated a beneficial effect by treating postmenopausal women with hormone replacement therapy,[11] although a recent update of the Women's Health Initiative examined age dependence and concluded that there were some beneficial effects of estrogen in younger women.[12] Taken together, these findings underscore the need for a better understanding of the mechanisms responsible for the male–female difference in HF.

Cardiac hypertrophy and HF have been associated with significant changes in the cardiac transcriptome, and altered expression of a number of mRNA transcripts and proteins have been associated with hypertrophy and HF.[13–17] It is clear, however, that complex diseases such as hypertrophy typically are caused not by alterations in a single mRNA or protein but rather by altered regulation of gene networks.[18,19] A systems biology approach to understand the development of and the sex differences in hypertrophy is needed. In this study, we used bioinformatics and systems biology approaches to identify mRNAs that

From the Systems Biology Center (J.H., N.F., A.S., J.Z., E.M.), System Biology Core (S.G., X.Z., Y.C., X.W.), DNA Sequencing & Genomics Core (Y.Y., P.L., J.Z.), and Murine Phenotyping Core (D.S.), National Heart, Lung and Blood Institute, National Institutes of Health, Bethesda, MD.

Accompanying Tables S1 through S5 and Figures S1 through S3 are available at http://jaha.ahajournals.org/content/6/8/e005838.full#sec-27.

*Dr Harrington, Dr Fillmore, Dr Gao, and Dr Yang contributed equally to this work.

Correspondence to: Elizabeth Murphy, PhD, NHLBI, NIH, Room 6N248B, Building 10, Bethesda, MD. E-mail: murphy1@mail.nih.gov

Received May 12, 2017; accepted June 21, 2017.

Clinical Perspective

What Is New?

- Although sex differences in the development of hypertrophy and heart failure are known, the mechanisms responsible are poorly understood.
- In this study, we used bioinformatics and systems biology approaches to identify mRNAs that were differentially expressed as a function of sex and hypertrophy and identified a role for PPARα (peroxisome proliferator-activated receptor α) in modulating the sex differences in hypertrophy.
- We find that PPARα is at the center of a network that is differentially regulated by sex and hypertrophy.

What Are the Clinical Implications?

- Better understanding the sex differences in the development of heart failure may lead to treatments targeting sex-specific patterns of cardiac maladaptation and damage.
- These data could have important implications for drugs used to treat hypertrophy.
- Understanding what protects women from heart failure could potentially allow us to offer the same protection to our male patients.

were differentially expressed as a function of sex and hypertrophy and identified a role for PPARα (peroxisome proliferator-activated receptor α) in modulating the sex differences in hypertrophy.

Methods

Mice

All mice were treated and cared for in accordance with the Guide for the Care and Use of Laboratory Animals (National Institutes of Health, revised 2011), and protocols were approved by the National Heart, Lung, and Blood Institute institutional animal care and use committee. Male and female C57BL/6 mice (12–14 weeks old, obtained from the Jackson Laboratory) were given angiotensin II at 1.5 mg/kg per day or saline (the vehicle) via Alzet minipumps for 2 or 3 weeks. In some studies, GW6471, a potent inhibitor of PPARα,[20] was also given at 4 mg/kg per day. GW6471 has an IC_{50} of 240 nmol/L and has been shown to function as an antagonist in mice within the range of 2 to 10 mg/kg per day.[21,22] Following treatment, echocardiography was performed on the mice. Mice were then anesthetized and euthanized. Their heart weights and tibia lengths were recorded, and harvested hearts were snap frozen and stored in liquid nitrogen.

2-Dimensional and M-Mode Echocardiography

Transthoracic echocardiography was performed using a high-frequency linear array ultrasound system (Vevo 2100, VisualSonics) and the MS-400 transducer (VisualSonics) with a center operating frequency of 30 MHz, broadband frequency of 18 to 38 MHz, axial resolution of 50 μm, and footprint of 20×5 mm. M-mode images of the left ventricle were collected from the parasternal short-axis view at the midpapillary muscles at a 90° clockwise rotation of the imaging probe from the parasternal long-axis view. From the M-mode images, the left ventricle systolic and diastolic posterior and anterior wall thicknesses and end-systolic and -diastolic internal left ventricle chamber dimensions were measured using the leading-edge method. Left ventricle functional values of fractional shortening and ejection fraction (EF) were calculated from the wall thicknesses and chamber dimension measurements using system software. Mice were lightly anesthetized with isoflurane delivered via a nose cone. The mice were imaged in the supine position while placed on a heated platform equipped with ECG leads.

RNA Extraction

0.5 mL TRI reagent was added to heart tissue along with Precellys (Bertin Technologies) homogenizing beads. Homogenization was carried out in a Precellys homogenizer (Bertin Technologies) chilled with liquid nitrogen. The samples were spun twice at 5000 rpm for 30 seconds for each cycle. RNA was isolated according to the TRI reagent protocol provided by Life Technologies. The isolated RNA samples were further cleaned with the miRNeasy Kit, according to the protocol provided by Qiagen. Samples were then treated with DNase (Ambion) and further cleaned with another Qiagen miRNeasy column. RNA concentration was determined by optical density at 260 nm.

RNA Sequencing Library Preparation and Statistical Analysis

The RNA sequencing libraries were constructed using a TruSeq Stranded Total RNA Sample Preparation Kit (Illumina), according to the manufacturer's protocols. Briefly, the ribosomal RNA was removed using Ribo-Zero (Illumina) rRNA removal beads. The resulting RNA was then fragmented using divalent cations under elevated temperature. The RNA fragments were copied into first-strand cDNA using reverse transcriptase and random hexamers. After second-strand synthesis, double-stranded cDNAs were ligated with Illumina adaptors. The final RNA sequencing library was enriched by low-cycle polymerase chain reaction and sequenced with paired 50-bp reads on an Illumina HiSeq 2000.

The raw data in fastq format were aligned to the mouse reference Ensembl GRCm38 genome using TopHat2[23] (tophat/2.0.13, Bowtie1/2.2.3, and samtools/0.1.19) with default settings except for the parameter –g 1. For transcript-level analysis, the raw counts of the transcripts in the mm10_refSeq.bed, which were produced by the software RSeQC/2.6, were used as the input for the Bioconductor edgeR package. TMM (Trimmed mean of M values) algorithms were used to normalize read counts across all 24 samples. The lowly expressed transcripts were discarded by requiring a count per million >1 in at least 3 samples. The euclidean distance metric was used for principal component analysis. The normalized and $\log_2$ transformed output count-per-million values were compared with a generalized linear model among 4 conditions. The differentially expressed transcripts were defined as ≥2-fold changes with a 10% false discovery rate (FDR).

For gene-level analysis, read counts were generated for each gene by HTSeq software[24] using the UCSC RefSeq annotation downloaded from iGenome in the "union" model. The statistical significance of differentially expressed genes was evaluated using edgeR.[25] The sex difference in hypertrophy was tested with edgeR's interaction (sex×disease) generalized linear model.

Functional enrichment analysis of differentially expressed transcripts was carried out using GOstats (https://www.bioconductor.org/packages/release/bioc/html/GOstats.html), and the results were summarized and visualized using REVIGO[26] (http://revigo.irb.hr/).

Transcription factor families whose binding sites were overrepresented in the promoter regions of the genes of interest were identified using Genomatix (https://www.genomatix.de/).

Coexpression Network Analysis

Coexpression networks shared in all 24 samples were constructed using the WGCNA package (weighted correlation network analysis, https://labs.genetics.ucla.edu/horvath/CoexpressionNetwork/Rpackages/WGCNA/).[27] WGCNA identifies robust clusters of highly correlated genes that serve as modules in coexpression networks and allows users to further examine correlation of network modules with experimental conditions and external traits. Global coexpression network construction is computationally intensive; therefore, to improve efficiency, we included only genes that showed differential expression at an FDR <10% and $|\log_2$ fold change$|>\log_2(1.2)$, in at least 1 of the 4 comparisons (baseline male and female, male control versus hypertrophy, female control versus hypertrophy, and male and female hypertrophy), totaling 4422 genes.

To examine the relevance to experimental conditions (sex and hypertrophy) of the resultant coexpression network modules, we constructed four 24-dimension condition-specific vectors (for male control, male hypertrophy, female control, and female hypertrophy, respectively). In the vectors, each element represents 1 sample, with a value of 1 if the sample belongs to the condition and 0 otherwise. The Pearson correlation between eigengenes of network modules and the condition vectors was then calculated for association estimation.

Protein–Protein Interaction Network Analysis and Subnetwork Identification

Protein–protein interaction annotation was downloaded from STRING (version 9),[28] a database of known and predicted protein–protein interactions (http://string-db.org/). Only interactions with a confidence score >700 were kept. Protein–protein interaction subnetworks with gene expression variations significantly associated with a factor (sex, hypertrophy, and the interaction between sex and hypertrophy) were identified using jActiveModulesTopo, a software package for trait-relevant subnetwork identification that takes network topology into consideration.[29]

Integrated Analysis of mRNA and MicroRNA Data

We developed a 3-step pipeline that determines regulatory relationships between microRNA (miRNA) and mRNA by integrating sequence-based prediction and experimental condition-dependent correlation in expression of miRNA and mRNA. First, TargetScan (http://www.targetscan.org/mmu_61/) was used to predict miRNA–mRNA regulatory relationships. TargetScan identified likely target mRNAs for each given miRNA by searching mRNAs for the presence of conserved sequence sites that matched the miRNA's seed regions. Second, correlation in expression variations of mRNA and miRNA were integrated with TargetScan predictions through Lasso (least absolute shrinkage and selection operator) regression to further narrow the list of candidate regulatory pairs. An R package developed by Lu et al[30] was used to carry out this step. Briefly, let y_i denote the expression level of the ith mRNA and $x_{k,i}$ the expression level of its k-th out of a total number (n) of candidate targeting miRNA in the simple linear regression model for y_i is given by:

$$y_i = \beta_{0,i} + \sum_{k=1}^{n} \beta_{k,i} x_{k,i} + \varepsilon_i \quad (1)$$

In equation (1), β represents the regression coefficients, and ε_i is a random error term. The lagrangian form of Lasso regression[31] of this model is as follows:

$$\left(\sum_{I=1}^{N} \left(y_i - \beta_{0,i} - \sum_{k=1}^{n} \beta_{k,i} x_{k,i} \right)^2 + \lambda \sum_{k=1}^{n} |\beta_{k,i}| \right) \quad (2)$$

In equation (2), λ is the lagrangian multiplier, and the regression is to find coefficients $\{\beta_{k,i}\}$ that minimize the value of equation (2). Lasso performs the regression with the sum of the absolute value of the regression coefficients constrained to balance between improving prediction accuracy and avoiding overfitting.

Third, the predicted miRNA–mRNA pairs were further filtered, and only those showing differential expression in 1 of the 3 statistical models—sex with hypertrophy controlled, hypertrophy with sex controlled, and the interaction between sex and hypertrophy—were retained. FDRs of 20% and 40% were used as the thresholds for mRNA and miRNA, respectively.

Results

Sex Differences in Angiotensin II–Induced Hypertrophy in Mice

Although previous studies have reported sex differences in hypertrophy,[6–8,32–35] the mechanistic basis for this difference is poorly understood. In this study, we measured global changes in mRNA and used a systems biology approach[18] to determine pathways and gene networks responsible for these sex differences. We first confirmed previous studies showing sex differences in hypertrophy. We initially treated male and female mice with angiotensin II for 3 weeks. As shown in Figure 1, after 3 weeks of angiotensin II treatment, male mice exhibited significantly more hypertrophy than female mice (Figure 1A). Furthermore, after 3 weeks of treatment, EF in female mice was not different compared with the control value (54% versus 56% at baseline). In male mice, however, EF dropped from the baseline level of 55% to 37% ($P<0.05$), which was significantly lower than EF in female mice after 3 weeks of treatment (Figure 1B). We also measured the percentage increase in aortic velocity (mean and peak) following angiotensin II treatment, and we observed similar increases in both male and female mice (36% increase in females and 29% increase in males).

We next used RNA sequencing to examine sex differences in mRNA at baseline and after 2 weeks of angiotensin II treatment. We measured mRNA after 2 weeks of treatment because at that time, sex differences in EF had not occurred (65±9% in females versus 61±9% in males, $P=0.53$, n=5–7). Thus, the changes in mRNA that occur at 2 weeks of treatment are more likely to be a cause rather than an effect of sex differences. Data were analyzed using pairwise comparisons of the conditions. As shown in Figure 2, principal component analysis revealed not only clustering differences between baseline and hypertrophy but also discrete clustering for mRNA of male and female mice at baseline that persisted following hypertrophy. The full data set

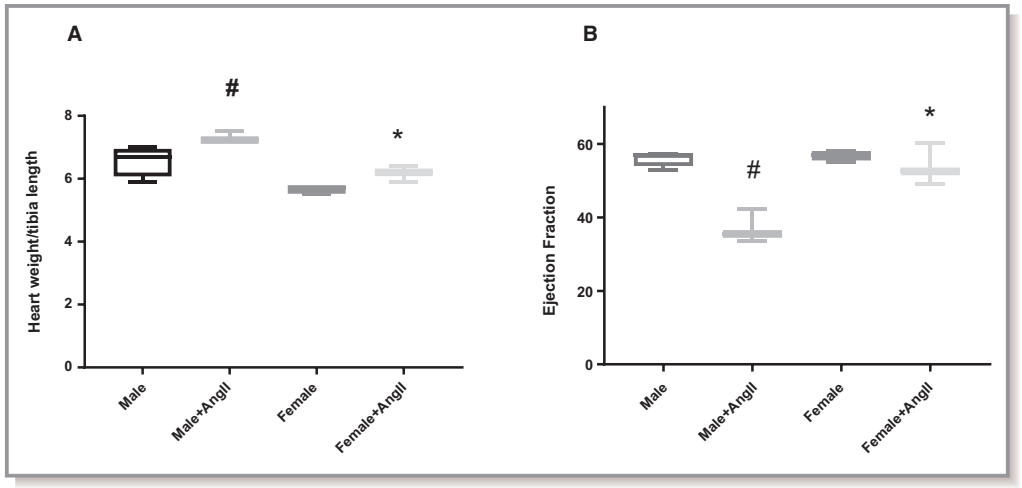

Figure 1. Sex differences in hypertrophy and ejection fraction following 3 weeks treatment with angiotensin II (AngII). Changes in (A) heart weight to tibia length and (B) ejection fraction in males and females following 3 weeks of AngII treatment. Data are mean±SEM, n=3 to 4. We performed a 2-way ANOVA. The heart weight/tibia length data showed significant differences based on sex and Ang II treatment, but there was not a significant interaction between sex and hypertrophy. The male vehicle-treated hearts were significantly different than male AngII-treated hearts, and male and female AngII-treated hearts were significantly different. The ejection fraction (EF) data showed a significant interaction between sex and hypertrophy. The males were significantly different between vehicle and AngII, and the males and females showed a significant difference with hypertrophy. #Significantly different compared with vehicle treated. *Significantly different from male Ang II treatment. $P<0.05$ was considered significant.

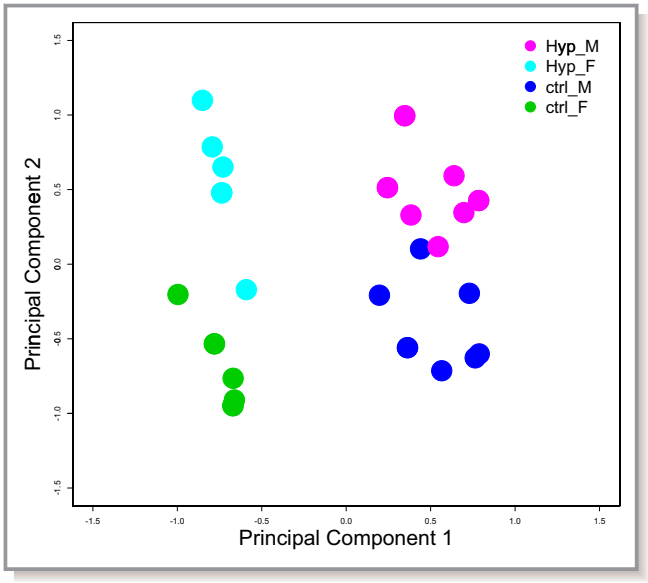

Figure 2. Principal component analysis for mRNA in male (M) and female (F) mice at baseline and with hypertrophy (Hyp), n=5 to 7 per group. Ctrl indicates control.

of mRNA, with significant changes, is provided in Table S1. The volcano plots in Figure 3 show differences in expression of mRNA between the groups. As illustrated in Figure 3A, comparing male and female mice at baseline, 174 transcripts showed a significant sex difference (using an FDR <10% and $\log_2$ fold change >1). Male mice tended to have more upregulated than downregulated genes compared with female mice (127 versus 47, respectively). Hypertrophy led to differential expression of mRNA in both male and female mice (Figure 3B through 3D). The mRNA changes that occur with hypertrophy largely overwhelm the baseline sex difference such that with hypertrophy, fewer mRNAs show a sex difference (compare Figure 3A and 3B). These differences are shown in more detail in the Venn diagram in Figure 4A. At an FDR <10% and $|\log_2(\text{fold change})|$ >1, there were 174 mRNAs (141 unique to baseline +33 overlapping with the list from hypertrophy) that exhibited a sex difference at baseline; however, following hypertrophy, only 71 mRNAs showed a sex difference, with 33 of these mRNAs showing a sex difference at both baseline and following hypertrophy. For the 141 transcripts that showed a sex difference only at baseline, 61 did not display a change with hypertrophy in either sex compared with their corresponding baselines, 10 displayed a hypertrophy-induced change in both sexes, 63 changed only in female hypertrophy, and 7 changed only in male hypertrophy.

If we examine differences between baseline and hypertrophy as a function of sex, we find that 328 mRNAs changed with hypertrophy in female mice, whereas only 174 mRNAs changed with hypertrophy in male mice. There are 117 mRNAs that changed in both male and female mice with hypertrophy; thus, 211 mRNAs are altered only in females with hypertrophy compared with 57 mRNAs that change only in males (see Figure 4B). Taken together, these data suggest that the process of hypertrophy overwhelms the sex differences observed at baseline.

To confirm the validity of our model, we confirmed an elevation in natriuretic peptide B (Figure 4C) and skeletal α-actin 1 (Figure 4D) with hypertrophy. Interestingly, although there were sex differences in the development of hypertrophy and in cardiac function following angiotensin II treatment, consistent with the RNA sequencing data, both male and female hearts showed significant increases in brain natriuretic peptide (Figure 4C). We found a similar discrepancy in a transaortic constriction model of hypertrophy in which we also observed a sex difference in hypertrophy but found no sex difference in natriuretic peptide B levels in heart.[6] We also confirmed the sex differences that were found in the transcriptomic analysis for metallothionein 1 and tissue metalloproteinase inhibitor 4 (see Figure S1).

Coexpression Network Analysis

Coexpression network analysis identifies gene sets showing significant and robust coregulations under the conditions of interest (hypertrophy and sex), manifested as modules in coexpression networks. Compared with the conventional pathway enrichment analysis that examines gene sets belonging to predefined pathways, it has the advantage of uncovering condition-specific gene signatures. In this study, we used WGCNA[27] to construct the coexpression network of the 4422 genes showing significant variations in response to sex, to hypertrophy, or to the interaction of sex and hypertrophy. Using all 24 samples, 20 coexpressed modules were identified. Figure 5 shows the module–condition correlation. The complete list of 4422 genes and their module memberships are given in Table S2. Coexpression network construction using gene lists filtered at other statistical stringencies or by variance in expression yielded similar module composition (data not shown).

The light yellow module with 25 mRNAs showed the most significant condition-specific differences along with the highest correlation and *P* value. At baseline, genes in this module were highly expressed in male but not in female mice. With hypertrophy, the sex difference diminished, and the genes were moderately expressed in both sexes. Consequently, this module displayed a sex difference in changes with hypertrophy. The module contained several mRNAs involved in metabolism including PPARα, Ccrn4l (carbon catabolite repression 4-like), Fitm1 (fat storage-inducing transmembrane domain 1), Acot1 (acyl–coenzyme A thioesterase 1), and Sik1 (salt inducible kinase 1). Several transcription factors (in addition to PPARα) and splicing factors were also

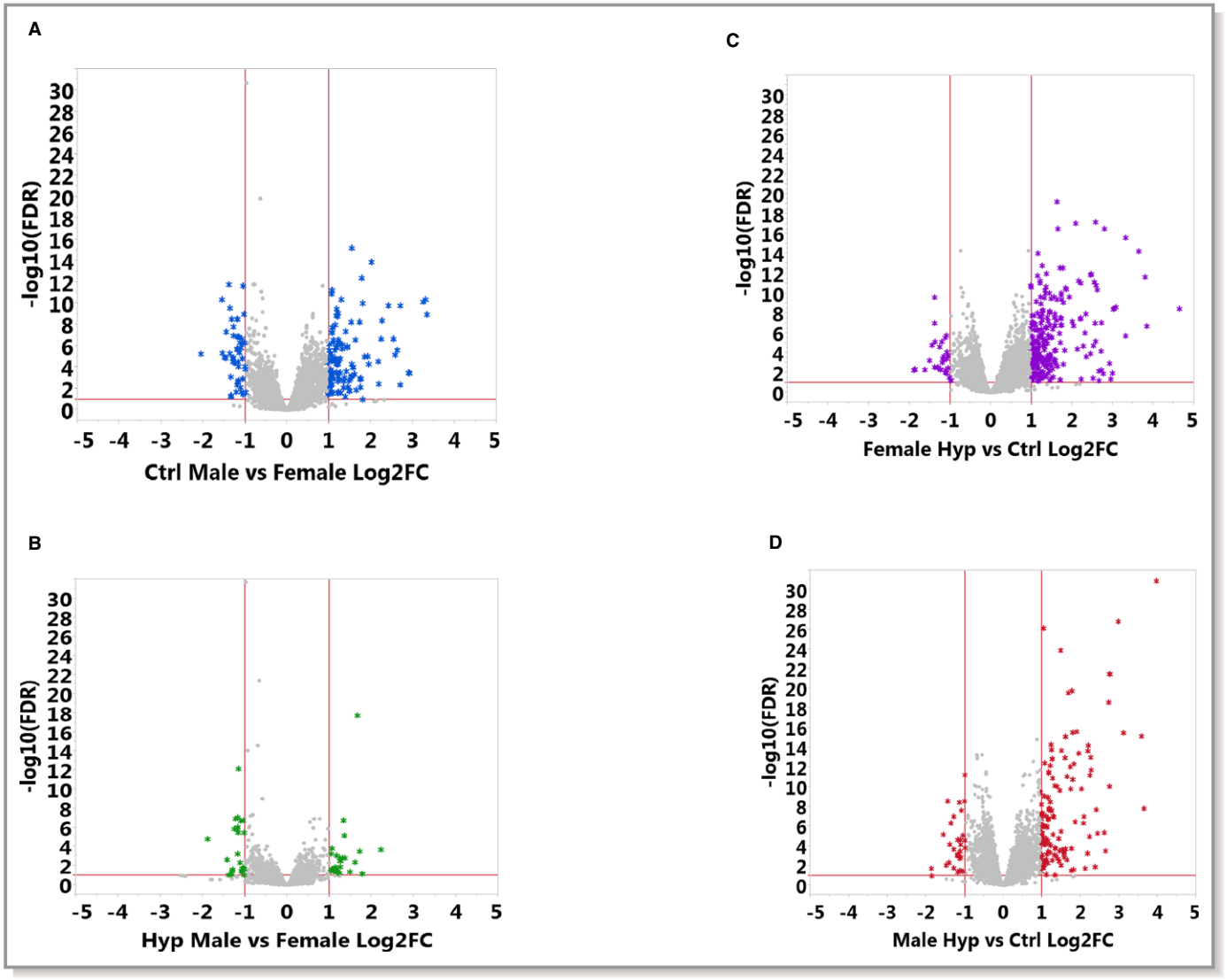

Figure 3. Volcano plots of mRNA differences. We used a filter of $\log_2$ fold change (FC) $\geq$1 and a false discovery rate (FDR) of 10% to select the transcripts with significant differences, which are shown in color. A, Data for mRNA in control (Ctrl) male vs female mice, with 174 transcripts (in blue) showing significant differences. B, 71 mRNA transcripts (in green) with significant differences between male and female hearts treated with angiotensin II (AngII). C, 328 transcripts (in purple) show significant differences in females with and without AngII treatment. D, 174 transcripts (in red) exhibit significant differences in males with and without AngII treatment. mRNA was measured in hearts from male and female mice treated with vehicle or AngII for 2 weeks. Hyp indicates hypertrophy.

contained in this module (Per1 [period circadian clock 1], SRSF3 [serine rich splicing factor 3], and Siah2 [siah E3 ubiquitin protein ligase 2]).

Interaction Model and Pathway Enrichment Analysis

To dissect the contributions from sex and hypertrophy and their interactions, we identified genes that showed significant changes in hypertrophy when sex as a cofactor was controlled, significant sex-dependent variation when hypertrophy as a cofactor was controlled, and significant sex-dependent differential hypertrophy-associated changes. This analysis was done at the gene level to avoid complications due to multiple splicing variants. At an FDR <40%, this approach gives 379 genes with significant interactions. The complete lists of genes with the statistics and pathway enrichment analysis results are available in Table S3. The pathway results were further simplified by removing redundancy in the tree-structured Gene Ontology terms and visualized using REVIGO (Figure 6). Four main categories were identified: cell-cycle and growth-related biosynthesis, cellular development process, extracellular matrix organization, and response to organic substances.

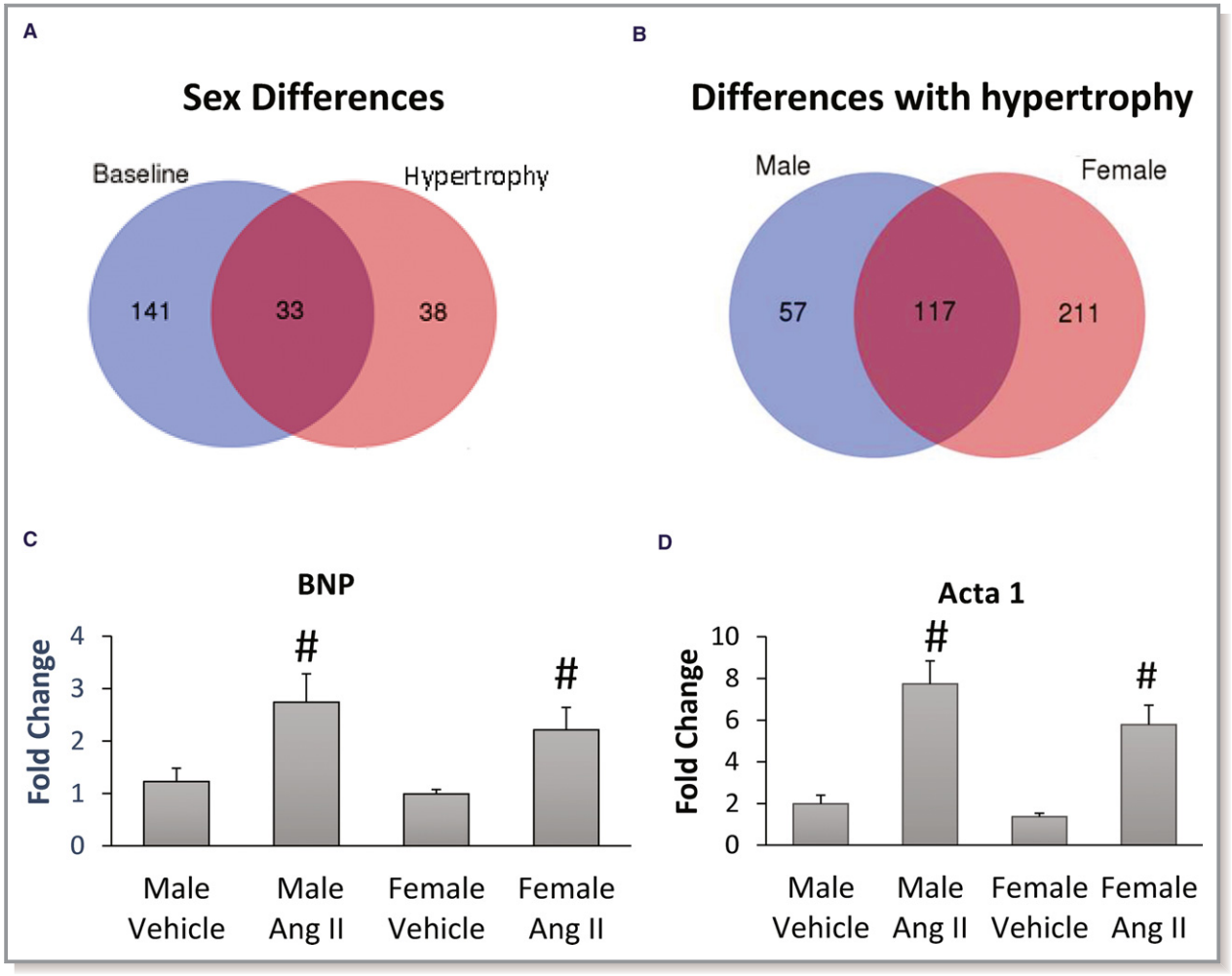

Figure 4. Sex differences in mRNA with angiotensin II (Ang II) treatment. The Venn diagram in (A) shows transcripts with significant sex differences at baseline and with Ang II treatment. Overall, 141 transcripts show differences only at baseline, 33 show differences at both baseline and hypertrophy, and 38 show a significant sex difference only with hypertrophy. B, Transcripts with a significant difference following Ang II treatment in males vs females. C, Quantitative polymerase chain reaction analysis showing changes in brain natriuretic peptide (BNP; mean and SEM) in fold change normalized to control males (n=5–7; #Significantly different compared with the vehicle control using 2-way ANOVA [$P<0.05$]).

Identification of a Gene Subnetwork That Is the Most Relevant to Sex-Dependent Difference in Hypertrophy-Induced Expression Changes

To gain further insight into the mRNA networks that played a role in the sex-dependent differences in hypertrophy-induced gene expression changes, we selected genes that were significant at an FDR <40% for the interaction and mapped them to the protein–protein interaction network constructed using STRING data. This provided a network with 178 genes and 313 interactions. We used an in-house software, jActiveModulesTopo[29,36] to identify the subnetworks that were most relevant to the sex–hypertrophy interaction (ie, connected sets of genes with high levels of sex–hypertrophy difference), using a simulated annealing method and setting the search depth at 2, and the result is given in Figure 7, with 17 genes and 22 interactions. This subnetwork is centered on PPARα, a clear hub with 8 interactions with other members, whereas the interactions for other genes ranged from 1 to 4. Note that PPARα is also implicated in the coexpression network analysis, being a member of a module that exhibited the most significant sex difference at baseline but not at hypertrophy (Figure 5, light yellow module).

PPARα has been shown previously to be involved in regulating hypertrophy.[37–42] Esrrg (estrogen-related receptor γ), a regulator of mitochondrial function that has been shown to play a role in regulating hypertrophy, is also found in this subnetwork. Intriguingly, a number of genes involved in circadian rhythms were also shown to have a sex and disease interaction; these include Per1, Arntl (aryl hydrocarbon receptor nuclear translocator-like protein 1; also known as Bmal [brain and muscle ARNT]), and Ccrn4ls. Among

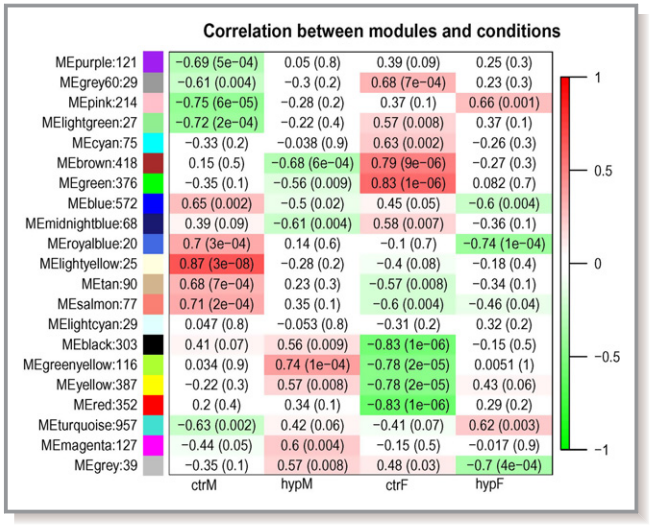

Figure 5. The 20 coexpression network modules shared by all samples and their correlation to experimental conditions. Each row corresponds to a module eigengene and each column to a condition. Each cell contains the corresponding Pearson correlation of the eigengene's expression and the condition vector, and in parentheses is the *P* value of the correlation. The table is color-coded by correlation value. Ctrl indicates control; F, female; hyp, hypertrophy, M, male.

them, Per1 and Ccrn4l were also members of the light yellow module shown in Figure 5. The expression levels of the key genes in this subnetwork that showed a sex bias are given in Figure S2. We also confirmed a sex difference in PPARα level with quantitative polymerase chain reaction (Figure S1).

Integrated Analysis of mRNA and miRNA

It is known that mRNAs are regulated in groups or networks by common transcriptional regulators, such as miRNAs; therefore, we performed an analysis of miRNAs on sham- and angiotensin II–treated male and female hearts after 2 weeks of treatment, using the same hearts that were used for mRNA measurement. The volcano plots illustrating miRNA differences between male and female hearts at baseline, male control and hypertrophy hearts, female control and hypertrophy hearts, and male and female hearts with hypertrophy are shown in Figure S3. The full data set is available in Table S4. Consistent with previous data in the literature and supporting the validity of the model, we found increases in miRNAs 15b, 21, 34, 199, 208b, and 214, which have all been reported previously to change with hypertrophic stimuli.[43–47]

We further performed an integrative analysis of mRNA–miRNA interaction. As described in the Methods, a Lasso regression model was used for identification of miRNA–mRNA targeting relationships that combine sequence-based prediction and experimental condition–dependent correlation in miRNA/mRNA expression variations. This was designed to overcome the problem of high false-positive rates in sequence-based predictions. This filtering with dynamic information of biological context-specific interactions improves reliability.

In total, TargetScan predicted 72 311 miRNA–mRNA targeting pairs, and less than one-third (23 323 pairs) remained after filtering with the Lasso regression. We then used cytoscape/Partek to generate a network of miRNA–mRNA targeting pairs most relevant to sex and hypertrophy interaction, as shown in Figure 7B. This analysis demonstrates sex and hypertrophy regulation of miRNAs 208b and 124. TargetScan shows miRNA 124 as a regulator of PPARα.

PPARα Inhibition Ameliorates Sex Difference in Hypertrophy

PPARα was found to be at the center of the network of mRNAs that were significantly different based on sex and hypertrophy (Figure 7); therefore, we examined whether PPARα contributes to sex differences in cardiac hypertrophy. To test whether PPARα regulates sex differences in hypertrophy, we examined whether inhibition of PPARα would block the sex differences observed with hypertrophic stimuli.

Cardiac hypertrophy was induced by treating male and female mice for 3 weeks with angiotensin II with and without GW6471, an inhibitor of PPARα. Consistent with the data in Figure 1, a sex difference in hypertrophy was observed with angiotensin II treatment (Figure 8). Interestingly, this sex difference in cardiac hypertrophy was blocked by treatment with GW6471 (Figure 8). These results are consistent with the hypothesis that PPARα contributes to sex differences in cardiac hypertrophy.

Discussion

Using a systems biology approach to explore sex differences in the cardiac transcriptome, we identified a genetic network surrounding PPARα that appears to be involved in the sexual dimorphism in cardiac hypertrophy. Most studies on hypertrophy focus on 1 or 2 mRNA or protein changes as the cause of hypertrophy, but it is becoming increasingly apparent that clusters of genes operating in networks play a role in regulating complex traits such as hypertrophy.[18] Because there are sex differences in the development of hypertrophy, it is reasonable to expect that sex differences in the regulation of these networks may contribute to sex differences in hypertrophy. Consistent with the concept that there are sex differences in the regulation of metabolic networks, metformin,[48] which is used to treat diabetes mellitus, has different effects on males and females.[49]

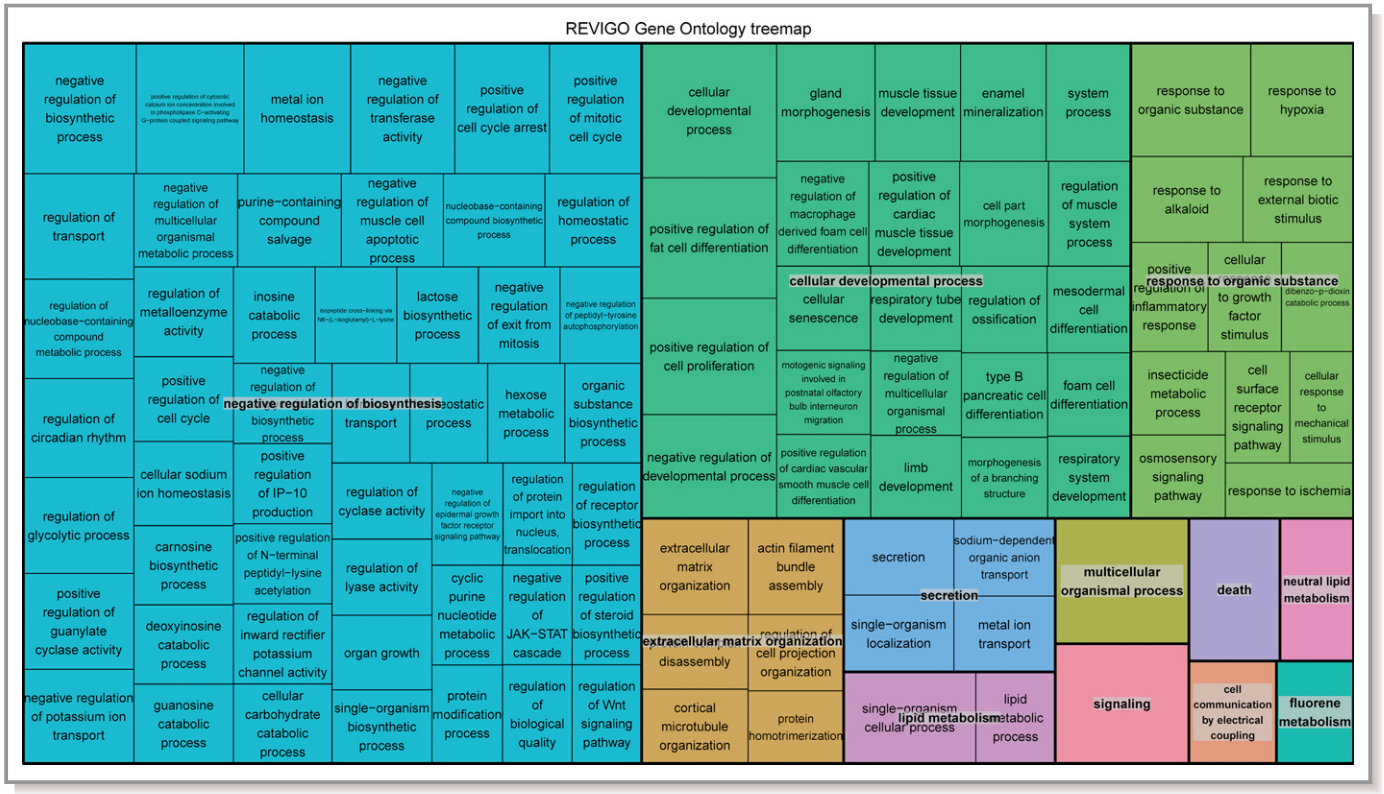

Figure 6. Pathways exhibiting alterations with sex and hypertrophy. Listed are pathways with enriched presence in genes that showed significant, sex-dependent differential hypertrophy-induced changes. This is a visualization of the results to help present the overall theme of the enriched pathways, in which the names in gray are representative and summarize pathway categories, and many redundant pathways are removed. IP-10 indicates chemokine (c-c motif) ligand 10.

To study sex differences in hypertrophy, we used a well-established model of angiotensin II–induced hypertrophy that was previously shown to be associated with estrogen-mediated differences in hypertrophy.[50] The mRNA was extracted from the whole heart, thus sex differences in cell-type composition could influence the result.

Consistent with previous studies, we found major sex differences in mRNAs at baseline.[51] A number of studies have examined transcriptome changes in hypertrophy; however, only a few studies have used a systems approach, and even fewer have looked at sex differences. Rau et al[13] used a systems genetic approach to identify gene pathways involved in isoproterenol-mediated hypertrophy and identified Adamts2 (ADAM metallopeptidase with thrombospondin type 1 motif 2) as a driver of isoproterenol-mediated hypertrophy. Interestingly, Adamts2 was found in the turquoise coexpression network module (see Figure 5). Park et al[14] used a genome-wide approach to identify pathways involved in hypertrophy; they found an increase in pathways involved in the immune response, extracellular matrix, and cell morphology in hypertrophy and a decrease in mitochondria and energy-producing pathways. Foster et al[15] examined the protein and mRNA changes in hypertrophy and found data suggesting a metabolic bottleneck in fatty acid oxidation. Drozdov et al[16] performed a similar coexpression network analysis to compare physiological and pathological hypertrophy. They reported major differences in network structure between physiological and pathological hypertrophy. Lai et al[17] performed transcriptomic and metabolic profiling in a hypertrophy model and an HF model in female mice. They reported that transcription and posttranscriptional changes in mitochondrial metabolic pathways in pressure overload induced HF. Sasagawa et al[52] compared 5 models of hypertrophic cardiomyopathy and found a consistent decrease in GSTK1 (glutathione S-transferase κ1). Taken together, the data in the literature suggest that hypertrophy involves changes in inflammation, fibrosis, metabolism, extracellular matrix, and ion channels. These data are consistent with our findings.

Only a few studies have examined sex differences in hypertrophy, and in contrast to our study, which used RNA sequencing, all of these studies used microarray chips to evaluate transcriptional changes. Heidecker et al[53] studied 29 men and 14 women with idiopathic dilated cardiomyopathy using the Affymetrix GeneChip. They reported that, compared with women, men exhibited an increase in 35 and a decrease in 16 transcripts. Many of these differences were

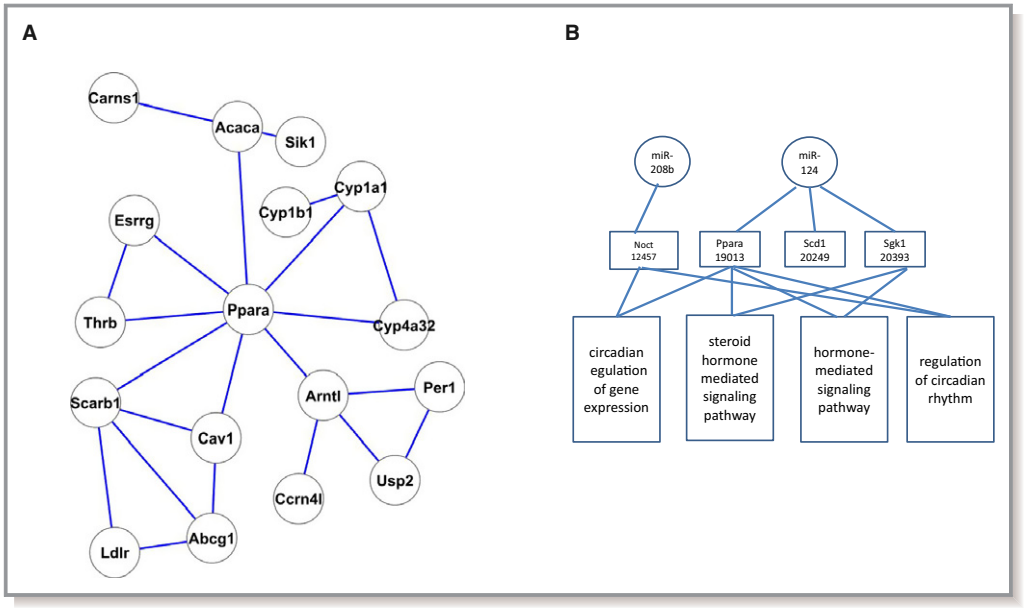

Figure 7. Network interactions. A, The top protein–protein interaction subnetwork associated with sex-dependent, hypertrophy-induced differential changes in gene expression are illustrated. B, Top microRNA–mRNA network relevant to sex–hypertrophy interaction.

on sex chromosomes. Kararigas et al[54] reported sex-dependent differences in transcripts in fibrosis and inflammation pathways in human pressure overload hypertrophy. Fermin et al[55] studied dilated cardiomyopathy in 30 female and 72 male patients and reported 1800 genes showing a sex difference, including genes in ion transport and G-protein–coupled receptor pathways. They also noted age dimorphisms in female but not in male patients. Sex- and age-dependent regulation of collagen has been reported in humans.[56] In young women, collagen types I and III are lower than in men, but with age, the trend reverses, and women have higher collagen I and III levels compared with men. Sex differences in collagen also occur during the development of hypertrophy. Michel et al reported that chronic isoproterenol stimulation in spontaneously hypertensive rats leads to an increase in collagen deposition in males but not in females.[57]

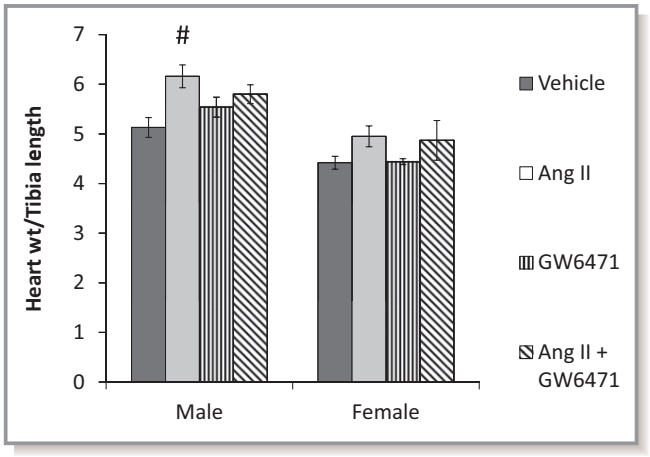

Figure 8. Inhibition of peroxisome proliferator-activated receptor α (PPARα) eliminates sex differences in cardiac hypertrophy. Angiotensin II (Ang II) and the PPARα inhibitor GW6471 (4 mg/kg per day) were administered for 3 weeks via osmotic minipumps, n=5 to 6. #Significantly different compared with the vehicle group. Values represented as mean±SEM. Significance was determined by ANOVA followed by a post hoc test. $P<0.05$ was considered significant.

Using a statistical analysis, we identified mRNA differences associated with sex and hypertrophy, and using STRING9, we built a gene interaction network to identify subnetworks that are likely to be involved in the difference in hypertrophy between males and females. As shown in Figure 7, PPARα, a well-established factor in hypertrophy,[37–41] is at the center of this hub. PPARα, a transcription factor that regulates metabolism, was previously reported to play a role in regulation of hypertrophy; however, it has not been implicated in sex differences in hypertrophy. During hypertrophy, the heart's metabolism shifts with an increase in glycolysis and a decreased reliance on fatty acid oxidation, consistent with a reversion to a fetal gene program with hypertrophy. Because PPARα is known to regulate fatty acid oxidation, it is not surprising that PPARα has been well documented to play a role in cardiac hypertrophy, although there is some disagreement as to whether it is beneficial or detrimental.[39] Most studies,[40,41] but not all,[42] report a decrease in PPARα with hypertrophy. Following hypertrophy, we found a decrease in PPARα in males but not in females (see Figure S2). It is possible that some of the discrepancy in the literature might

be explained by this sex difference. The effects of increased or decreased levels or activity of PPARα are complex, and depending on the conditions, both can enhance hypertrophy. Addition of fenofibrate, a PPARα agonist, has been shown to reduce hypertrophy.[58,59] In contrast, treatment with a different PPARα agonist, WY-14643 did not reduce cardiac hypertrophy and resulted in increased contractile dysfunction.[41] In addition, mice with cardiac-specific transgenic overexpression of PPARα develop cardiac hypertrophy and a phenotype similar to that seen with diabetic cardiomyopathy.[38]

Hypertrophy has also been assessed in mice with a global deletion of PPARα. Consistent with a role for PPARα in regulating fatty acid oxidation, PPARα-knockout mice have a decrease in fatty acid oxidation. Most studies report no baseline dysfunction in PPARα-knockout mice.[60] Oka et al[42] reported that haplosufficiency of PPARα attenuated pressure overload–induced hypertrophy. Taken together, the data suggest that dysregulation of PPARα can modulate the development of hypertrophy. It appears, however, that there is a "sweet spot" for PPARα levels or activity; too much or too little PPARα can lead to hypertrophy. The data in Figure 7 suggest that sex differences in PPARα are involved in sex differences in hypertrophy. This hypothesis would be consistent with data showing sex differences in the regulation of PPARα.[61–63] Of note in PPARα-knockout mice, inhibition of carnitine palmitoyltransferase I resulted in death of 100% of the male mice but only 25% of the female mice, suggesting sex differences in the response to changes in PPARα.[64] We reasoned that if PPARα mediates the sex difference in hypertrophy, elimination of sex differences in PPARα using an acute 3-week treatment with an inhibitor should block the sex differences in the development of hypertrophy. Because adaptive changes can occur during global loss of PPARα, we used an inhibitor to acutely inhibit PPARα. In support of a role of PPARα in mediating sex differences in hypertrophy, we found that 3 weeks of treatment with a PPARα antagonist eliminated the sex difference in hypertrophy. These data support the concept that this PPARα-centered network is involved in sex differences in hypertrophy; however, given the established role of PPARα in regulating hypertrophy, it is not surprising that inhibition of PPARα blocks hypertrophy in males. Because both inhibition and overexpression of PPARα can increase hypertrophy, it is difficult to unambiguously test its role in sex differences.

Although the sex- and hypertrophy-dependent network in Figure 7 is centered on PPARα, other known regulators of cardiac hypertrophy are also involved, including ESRRG. ESRRG is activated by PGC-1α (PPARγ coactivator 1α) and PGC-1β and has been shown to coordinate with PPARα to regulate myocardial metabolism and hypertrophy. PPARα is known to be involved in circadian regulation of metabolism, and BMAL1 (also known as nocturnin), which is a component of circadian regulation and regulates metabolism,[65] is also involved in this network. PPARα has been shown to bind to a response element on the BMAL1 promoter; in turn, BMAL1 is an upstream regulator of PPARα expression.[66] Cardiac-specific deletion of BMAL leads to altered metabolism and development of cardiomyopathy with aging.[67] BMAL1 forms a heterodimer with CLOCK (clock circadian regulator), which regulates Per1, shown in Figure 7 to be a component of this sex and hypertrophy regulated network. Interestingly, BMAL1 regulates Ccrn4l, which is also a member of the network in Figure 7. These data are consistent with an emerging body of literature showing sex differences in circadian regulation.

These data raise the question of what mediates the differential regulation of this network. Because networks are typically regulated by common transcription factors or common epigenetic signals, we considered whether transcription factors might be involved in the differential regulation of the network. The transcription factor binding-site family of KLF (Kruppel-like factor) transcription factors was overrepresented and showed a high Z-score on promoters of genes significant for sex–hypertrophy interaction (see Table S5). Some KLF transcription factors are reported to regulate PPARα,[68] and KLF family members and PPAR exhibit circadian regulation,[69–71] making them potential candidates. KLF4 has also been shown to cooperate with ESRR and PGC-1 to regulate mitochondrial function and metabolism.[72]

We also observed a sex- and hypertrophy-dependent difference in miR208b. miR208b is contained in an intron of Myh7, and miR208a, which has close homology with miR208b, is generated from an intron of Myh6.[73] In mice, Myh7 is the cardiac fetal isoform, and after birth, the heart switches to Myh6. With hypertrophy, there is a switch from Myh6 back to the fetal isoform Myh7 and a concomitant increase in miR208b.[74,75] Mechanical stress and hypothyroidism result in a shift from Myh6 to Myh7, and this shift requires miR208a. When miR208a is deleted, stress or hypothyroidism no longer leads to upregulation of Myh7. Although an increase in miR208b has been reported to occur with hypertrophy, there are no reports on sex differences. PPARα and ESRRG were recently shown to regulate the skeletal muscle fiber type switch to Myh7.[76] ESRRG was shown to activate, whereas PPARα inhibited miR208b, and miR449 mediated upregulation of Myh7.[76] Whether a similar program is present in the heart is unclear.

In summary, we find that PPARα is at the center of a network that is differentially regulated by sex and hypertrophy. We further demonstrate that acute inhibition of PPARα blocks the sex difference in hypertrophy. Many of the mRNAs regulated by sex and hypertrophy were previously shown to be involved in hypertrophy, although sex differences in their signaling have not been examined. The data in our study suggest that the network in Figure 7 is differentially

regulated in hypertrophy and that this differential regulation leads to sex differences in hypertrophy. These data could have important implications for drugs used to treat hypertrophy.

Sources of Funding

All investigators in this study were funded by the intramural program of the National Heart, Lung, and Blood Institute of National Institutes of Health.

Disclosures

None.

References

1. Barrett-Connor E. Sex differences in coronary heart disease. Why are women so superior? The 1995 Ancel Keys Lecture. *Circulation*. 1997;95:252–264.
2. Hayward CS, Kelly RP, Collins P. The roles of gender, the menopause and hormone replacement on cardiovascular function. *Cardiovasc Res*. 2000;46:28–49.
3. Krumholz HM, Larson M, Levy D. Sex differences in cardiac adaptation to isolated systolic hypertension. *Am J Cardiol*. 1993;72:310–313.
4. Lee DS, Gona P, Vasan RS, Larson MG, Benjamin EJ, Wang TJ, Tu JV, Levy D. Relation of disease pathogenesis and risk factors to heart failure with preserved or reduced ejection fraction: insights from the Framingham Heart Study of the National Heart, Lung, and Blood Institute. *Circulation*. 2009;119:3070–3077.
5. Scantlebury DC, Borlaug BA. Why are women more likely than men to develop heart failure with preserved ejection fraction? *Curr Opin Cardiol*. 2011;26:562–568.
6. Skavdahl M, Steenbergen C, Clark J, Myers P, Demianenko T, Mao L, Rockman HA, Korach KS, Murphy E. Estrogen receptor-beta mediates male-female differences in the development of pressure overload hypertrophy. *Am J Physiol Heart Circ Physiol*. 2005;288:H469–H476.
7. Dash R, Schmidt AG, Pathak A, Gerst MJ, Biniakiewicz D, Kadambi VJ, Hoit BD, Abraham WT, Kranias EG. Differential regulation of p38 mitogen-activated protein kinase mediates gender-dependent catecholamine-induced hypertrophy. *Cardiovasc Res*. 2003;57:704–714.
8. Douglas PS, Katz SE, Weinberg EO, Chen MH, Bishop SP, Lorell BH. Hypertrophic remodeling: gender differences in the early response to left ventricular pressure overload. *J Am Coll Cardiol*. 1998;32:1118–1125.
9. Kadokami T, McTiernan CF, Kubota T, Frye CS, Feldman AM. Sex-related survival differences in murine cardiomyopathy are associated with differences in TNF-receptor expression. *J Clin Invest*. 2000;106:589–597.
10. Stauffer BL, Dockstader K, Russell G, Hijmans J, Walker L, Cecil M, Demos-Davies K, Medway A, McKinsey TA, Sucharov CC. Transgenic over-expression of YY1 induces pathologic cardiac hypertrophy in a sex-specific manner. *Biochem Biophys Res Commun*. 2015;462:131–137.
11. Rossouw JE, Anderson GL, Prentice RL, LaCroix AZ, Kooperberg C, Stefanick ML, Jackson RD, Beresford SA, Howard BV, Johnson KC, Kotchen JM, Ockene J; Writing Group for the Women's Health Initiative I. Risks and benefits of estrogen plus progestin in healthy postmenopausal women: principal results from the Women's Health Initiative randomized controlled trial. *JAMA*. 2002;288:321–333.
12. Manson JE, Chlebowski RT, Stefanick ML, Aragaki AK, Rossouw JE, Prentice RL, Anderson G, Howard BV, Thomson CA, LaCroix AZ, Wactawski-Wende J, Jackson RD, Limacher M, Margolis KL, Wassertheil-Smoller S, Beresford SA, Cauley JA, Eaton CB, Gass M, Hsia J, Johnson KC, Kooperberg C, Kuller LH, Lewis CE, Liu S, Martin LW, Ockene JK, O'Sullivan MJ, Powell LH, Simon MS, Van Horn L, Vitolins MZ, Wallace RB. Menopausal hormone therapy and health outcomes during the intervention and extended poststopping phases of the Women's Health Initiative randomized trials. *JAMA*. 2013;310:1353–1368.
13. Rau CD, Romay MC, Tuteryan M, Wang JJ, Santolini M, Ren S, Karma A, Weiss JN, Wang Y, Lusis AJ. Systems genetics approach identifies gene pathways and Adamts2 as drivers of isoproterenol-induced cardiac hypertrophy and cardiomyopathy in mice. *Cell Syst*. 2017;4:121–128.e4.
14. Park JY, Li W, Zheng D, Zhai P, Zhao Y, Matsuda T, Vatner SF, Sadoshima J, Tian B. Comparative analysis of mRNA isoform expression in cardiac hypertrophy and development reveals multiple post-transcriptional regulatory modules. *PLoS One*. 2011;6:e22391.
15. Foster DB, Liu T, Kammers K, O'Meally R, Yang N, Papanicolaou KN, Talbot CC Jr, Cole RN, O'Rourke B. Integrated omic analysis of a guinea pig model of heart failure and sudden cardiac death. *J Proteome Res*. 2016;15:3009–3028.
16. Drozdov I, Didangelos A, Yin X, Zampetaki A, Abonnenc M, Murdoch C, Zhang M, Ouzounis CA, Mayr M, Tsoka S, Shah AM. Gene network and proteomic analyses of cardiac responses to pathological and physiological stress. *Circ Cardiovasc Genet*. 2013;6:588–597.
17. Lai L, Leone TC, Keller MP, Martin OJ, Broman AT, Nigro J, Kapoor K, Koves TR, Stevens R, Ilkayeva OR, Vega RB, Attie AD, Muoio DM, Kelly DP. Energy metabolic reprogramming in the hypertrophied and early stage failing heart: a multisystems approach. *Circ Heart Fail*. 2014;7:1022–1031.
18. MacLellan WR, Wang Y, Lusis AJ. Systems-based approaches to cardiovascular disease. *Nat Rev Cardiol*. 2012;9:172–184.
19. Weiss JN, Karma A, MacLellan WR, Deng M, Rau CD, Rees CM, Wang J, Wisniewski N, Eskin E, Horvath S, Qu Z, Wang Y, Lusis AJ. "Good enough solutions" and the genetics of complex diseases. *Circ Res*. 2012;111:493–504.
20. Xu HE, Stanley TB, Montana VG, Lambert MH, Shearer BG, Cobb JE, McKee DD, Galardi CM, Plunket KD, Nolte RT, Parks DJ, Moore JT, Kliewer SA, Willson TM, Stimmel JB. Structural basis for antagonist-mediated recruitment of nuclear co-repressors by PPARalpha. *Nature*. 2002;415:813–817.
21. Jackson A, Bagdas D, Muldoon PP, Lichtman AH, Carroll FI, Greenwald M, Miles MF, Damaj MI. In vivo interactions between alpha7 nicotinic acetylcholine receptor and nuclear peroxisome proliferator-activated receptor-alpha: implication for nicotine dependence. *Neuropharmacology*. 2017;118:38–45.
22. Cermenati G, Audano M, Giatti S, Carozzi V, Porretta-Serapiglia C, Pettinato E, Ferri C, D'Antonio M, De Fabiani E, Crestani M, Scurati S, Saez E, Azcoitia I, Cavaletti G, Garcia-Segura LM, Melcangi RC, Caruso D, Mitro N. Lack of sterol regulatory element binding factor-1c imposes glial fatty acid utilization leading to peripheral neuropathy. *Cell Metab*. 2015;21:571–583.
23. Kim D, Pertea G, Trapnell C, Pimentel H, Kelley R, Salzberg SL. Tophat2: Accurate alignment of transcriptomes in the presence of insertions, deletions and gene fusions. *Genome Biol*. 2013;14:R36.
24. Anders S, Pyl PT, Huber W. Htseq–a python framework to work with high-throughput sequencing data. *Bioinformatics*. 2015;31:166–169.
25. Robinson MD, McCarthy DJ, Smyth GK. Edger: A bioconductor package for differential expression analysis of digital gene expression data. *Bioinformatics*. 2010;26:139–140.
26. Supek F, Bosnjak M, Skunca N, Smuc T. REVIGO summarizes and visualizes long lists of gene ontology terms. *PLoS One*. 2011;6:e21800.
27. Langfelder P, Horvath S. WGCNA: an R package for weighted correlation network analysis. *BMC Bioinformatics*. 2008;9:559.
28. von Mering C, Jensen LJ, Snel B, Hooper SD, Krupp M, Foglierini M, Jouffre N, Huynen MA, Bork P. STRING: known and predicted protein-protein associations, integrated and transferred across organisms. *Nucleic Acids Res*. 2005;33:D433–D437.
29. Gao SG, Jia S, Hessner MJ, Wang XJ. Predicting disease-related subnetworks for type 1 diabetes using a new network activity score. *OMICS*. 2012;16:566–578.
30. Lu Y, Zhou Y, Qu W, Deng M, Zhang C. A Lasso regression model for the construction of microRNA-target regulatory networks. *Bioinformatics*. 2011;27:2406–2413.
31. Tibshirani R. Regression shrinkage and selection via the Lasso. *J R Stat Soc Series B Methodol*. 1996;58:267–288.
32. Levy D, Anderson KM, Savage DD, Kannel WB, Christiansen JC, Castelli WP. Echocardiographically detected left ventricular hypertrophy: prevalence and risk factors. The Framingham Heart Study. *Ann Intern Med*. 1988;108:7–13.
33. Olsson MC, Palmer BM, Leinwand LA, Moore RL. Gender and aging in a transgenic mouse model of hypertrophic cardiomyopathy. *Am J Physiol Heart Circ Physiol*. 2001;280:H1136–H1144.
34. Fischer TH, Herting J, Eiringhaus J, Pabel S, Hartmann NH, Ellenberger D, Friedrich M, Renner A, Gummert J, Maier LS, Zabel M, Hasenfuss G, Sossalla S. Sex-dependent alterations of Ca^{2+} cycling in human cardiac hypertrophy and heart failure. *Europace*. 2016;18:1440–1448.
35. Janicki JS, Spinale FG, Levick SP. Gender differences in non-ischemic myocardial remodeling: are they due to estrogen modulation of cardiac mast cells and/or membrane type 1 matrix metalloproteinase. *Pflugers Arch*. 2013;465:687–697.
36. Gao S, Wang X. Predicting type 1 diabetes candidate genes using human protein-protein interaction networks. *J Comput Sci Syst Biol*. 2009;2:133.

37. Smeets PJ, Teunissen BE, Willemsen PH, van Nieuwenhoven FA, Brouns AE, Janssen BJ, Cleutjens JP, Staels B, van der Vusse GJ, van Bilsen M. Cardiac hypertrophy is enhanced in PPAR alpha-/- mice in response to chronic pressure overload. *Cardiovasc Res*. 2008;78:79–89.
38. Finck BN, Lehman JJ, Leone TC, Welch MJ, Bennett MJ, Kovacs A, Han X, Gross RW, Kozak R, Lopaschuk GD, Kelly DP. The cardiac phenotype induced by PPARalpha overexpression mimics that caused by diabetes mellitus. *J Clin Invest*. 2002;109:121–130.
39. Pol CJ, Lieu M, Drosatos K. PPARs: protectors or opponents of myocardial function? *PPAR Res*. 2015;2015:835985.
40. Barger PM, Brandt JM, Leone TC, Weinheimer CJ, Kelly DP. Deactivation of peroxisome proliferator-activated receptor-alpha during cardiac hypertrophic growth. *J Clin Invest*. 2000;105:1723–1730.
41. Young ME, Laws FA, Goodwin GW, Taegtmeyer H. Reactivation of peroxisome proliferator-activated receptor alpha is associated with contractile dysfunction in hypertrophied rat heart. *J Biol Chem*. 2001;276:44390–44395.
42. Oka S, Alcendor R, Zhai P, Park JY, Shao D, Cho J, Yamamoto T, Tian B, Sadoshima J. PPARalpha-Sirt1 complex mediates cardiac hypertrophy and failure through suppression of the ERR transcriptional pathway. *Cell Metab*. 2011;14:598–611.
43. Small EM, Frost RJ, Olson EN. MicroRNAs add a new dimension to cardiovascular disease. *Circulation*. 2010;121:1022–1032.
44. Hullinger TG, Montgomery RL, Seto AG, Dickinson BA, Semus HM, Lynch JM, Dalby CM, Robinson K, Stack C, Latimer PA, Hare JM, Olson EN, van Rooij E. Inhibition of miR-15 protects against cardiac ischemic injury. *Circ Res*. 2012;110:71–81.
45. Yang Y, Cheng HW, Qiu Y, Dupee D, Noonan M, Lin YD, Fisch S, Unno K, Sereti KI, Liao R. MicroRNA-34a plays a key role in cardiac repair and regeneration following myocardial infarction. *Circ Res*. 2015;117:450–459.
46. Dorn GW II. MicroRNAs in cardiac disease. *Transl Res*. 2011;157:226–235.
47. Da Costa Martins PA, De Windt LJ. MicroRNAs in control of cardiac hypertrophy. *Cardiovasc Res*. 2012;93:563–572.
48. Lyons MR, Peterson LR, McGill JB, Herrero P, Coggan AR, Saeed IM, Recklein C, Schechtman KB, Gropler RJ. Impact of sex on the heart's metabolic and functional responses to diabetic therapies. *Am J Physiol Heart Circ Physiol*. 2013;305:H1584–H1591.
49. Murphy E, Steenbergen C. Sex, drugs, and trial design: sex influences the heart and drug responses. *J Clin Invest*. 2014;124:2375–2377.
50. Pedram A, Razandi M, Lubahn D, Liu J, Vannan M, Levin ER. Estrogen inhibits cardiac hypertrophy: role of estrogen receptor-beta to inhibit calcineurin. *Endocrinology*. 2008;149:3361–3369.
51. Queiros AM, Eschen C, Fliegner D, Kararigas G, Dworatzek E, Westphal C, Sanchez Ruderisch H, Regitz-Zagrosek V. Sex- and estrogen-dependent regulation of a miRNA network in the healthy and hypertrophied heart. *Int J Cardiol*. 2013;169:331–338.
52. Sasagawa S, Nishimura Y, Okabe S, Murakami S, Ashikawa Y, Yuge M, Kawaguchi K, Kawase R, Okamoto R, Ito M, Tanaka T. Downregulation of GSTK1 is a common mechanism underlying hypertrophic cardiomyopathy. *Front Pharmacol*. 2016;7:162.
53. Heidecker B, Lamirault G, Kasper EK, Wittstein IS, Champion HC, Breton E, Russell SD, Hall J, Kittleson MM, Baughman KL, Hare JM. The gene expression profile of patients with new-onset heart failure reveals important gender-specific differences. *Eur Heart J*. 2010;31:1188–1196.
54. Kararigas G, Dworatzek E, Petrov G, Summer H, Schulze TM, Baczko I, Knosalla C, Golz S, Hetzer R, Regitz-Zagrosek V. Sex-dependent regulation of fibrosis and inflammation in human left ventricular remodelling under pressure overload. *Eur J Heart Fail*. 2014;16:1160–1167.
55. Fermin DR, Barac A, Lee S, Polster SP, Hannenhalli S, Bergemann TL, Grindle S, Dyke DB, Pagani F, Miller LW, Tan S, Dos Remedios C, Cappola TP, Margulies KB, Hall JL. Sex and age dimorphism of myocardial gene expression in nonischemic human heart failure. *Circ Cardiovasc Genet*. 2008;1:117–125.
56. Dworatzek E, Baczko I, Kararigas G. Effects of aging on cardiac extracellular matrix in men and women. *Proteomics Clin Appl*. 2016;10:84–91.
57. Michel FS, Magubane M, Mokotedi L, Norton GR, Woodiwiss AJ. Sex-specific effects of adrenergic-induced left ventricular remodeling in spontaneously hypertensive rats. *J Card Fail*. 2017;23:161–168.
58. Duhaney TA, Cui L, Rude MK, Lebrasseur NK, Ngoy S, De Silva DS, Siwik DA, Liao R, Sam F. Peroxisome proliferator-activated receptor alpha-independent actions of fenofibrate exacerbates left ventricular dilation and fibrosis in chronic pressure overload. *Hypertension*. 2007;49:1084–1094.
59. Zou J, Le K, Xu S, Chen J, Liu Z, Chao X, Geng B, Luo J, Zeng S, Ye J, Liu P. Fenofibrate ameliorates cardiac hypertrophy by activation of peroxisome proliferator-activated receptor-alpha partly via preventing p65-NFkappaB binding to NFATc4. *Mol Cell Endocrinol*. 2013;370:103–112.
60. Luptak I, Balschi JA, Xing Y, Leone TC, Kelly DP, Tian R. Decreased contractile and metabolic reserve in peroxisome proliferator-activated receptor-alpha-null hearts can be rescued by increasing glucose transport and utilization. *Circulation*. 2005;112:2339–2346.
61. Wege N, Schutkowski A, Boenn M, Bialek J, Schlitt A, Noack F, Grosse I, Stangl GI. Men and women differ in their diurnal expression of monocyte peroxisome proliferator-activated receptor-alpha in the fed but not in the fasted state. *FASEB J*. 2015;29:2905–2911.
62. Essop MF, Chan WY, Taegtmeyer H. Metabolic gene switching in the murine female heart parallels enhanced mitochondrial respiratory function in response to oxidative stress. *FEBS J*. 2007;274:5278–5284.
63. Dotson AL, Wang J, Chen Y, Manning D, Nguyen H, Saugstad JA, Offner H. Sex differences and the role of PPAR alpha in experimental stroke. *Metab Brain Dis*. 2016;31:539–547.
64. Djouadi F, Weinheimer CJ, Saffitz JE, Pitchford C, Bastin J, Gonzalez FJ, Kelly DP. A gender-related defect in lipid metabolism and glucose homeostasis in peroxisome proliferator- activated receptor alpha- deficient mice. *J Clin Invest*. 1998;102:1083–1091.
65. Stubblefield JJ, Terrien J, Green CB. Nocturnin: at the crossroads of clocks and metabolism. *Trends Endocrinol Metab*. 2012;23:326–333.
66. Canaple L, Rambaud J, Dkhissi-Benyahya O, Rayet B, Tan NS, Michalik L, Delaunay F, Wahli W, Laudet V. Reciprocal regulation of brain and muscle Arnt-like protein 1 and peroxisome proliferator-activated receptor alpha defines a novel positive feedback loop in the rodent liver circadian clock. *Mol Endocrinol*. 2006;20:1715–1727.
67. Young ME, Brewer RA, Peliciari-Garcia RA, Collins HE, He L, Birky TL, Peden BW, Thompson EG, Ammons BJ, Bray MS, Chatham JC, Wende AR, Yang Q, Chow CW, Martino TA, Gamble KL. Cardiomyocyte-specific BMAL1 plays critical roles in metabolism, signaling, and maintenance of contractile function of the heart. *J Biol Rhythms*. 2014;29:257–276.
68. Drosatos K, Pollak NM, Pol CJ, Ntziachristos P, Willecke F, Valenti MC, Trent CM, Hu Y, Guo S, Aifantis I, Goldberg IJ. Cardiac myocyte KLF5 regulates Ppara expression and cardiac function. *Circ Res*. 2016;118:241–253.
69. Jeyaraj D, Haldar SM, Wan X, McCauley MD, Ripperger JA, Hu K, Lu Y, Eapen BL, Sharma N, Ficker E, Cutler MJ, Gulick J, Sanbe A, Robbins J, Demolombe S, Kondratov RV, Shea SA, Albrecht U, Wehrens XH, Rosenbaum DS, Jain MK. Circadian rhythms govern cardiac repolarization and arrhythmogenesis. *Nature*. 2012;483:96–99.
70. Schmutz I, Ripperger JA, Baeriswyl-Aebischer S, Albrecht U. The mammalian clock component PERIOD2 coordinates circadian output by interaction with nuclear receptors. *Genes Dev*. 2010;24:345–357.
71. Lecarpentier Y, Claes V, Duthoit G, Hebert JL. Circadian rhythms, Wnt/beta-catenin pathway and PPAR alpha/gamma profiles in diseases with primary or secondary cardiac dysfunction. *Front Physiol*. 2014;5:429.
72. Liao X, Zhang R, Lu Y, Prosdocimo DA, Sangwung P, Zhang L, Zhou G, Anand P, Lai L, Leone TC, Fujioka H, Ye F, Rosca MG, Hoppel CL, Schulze PC, Abel ED, Stamler JS, Kelly DP, Jain MK. Kruppel-like factor 4 is critical for transcriptional control of cardiac mitochondrial homeostasis. *J Clin Invest*. 2015;125:3461–3476.
73. van Rooij E, Quiat D, Johnson BA, Sutherland LB, Qi X, Richardson JA, Kelm RJ Jr, Olson EN. A family of microRNAs encoded by myosin genes governs myosin expression and muscle performance. *Dev Cell*. 2009;17:662–673.
74. Montgomery RL, Hullinger TG, Semus HM, Dickinson BA, Seto AG, Lynch JM, Stack C, Latimer PA, Olson EN, van Rooij E. Therapeutic inhibition of miR-208a improves cardiac function and survival during heart failure. *Circulation*. 2011;124:1537–1547.
75. van Rooij E, Sutherland LB, Qi X, Richardson JA, Hill J, Olson EN. Control of stress-dependent cardiac growth and gene expression by a microRNA. *Science*. 2007;316:575–579.
76. Gan Z, Rumsey J, Hazen BC, Lai L, Leone TC, Vega RB, Xie H, Conley KE, Auwerx J, Smith SR, Olson EN, Kralli A, Kelly DP. Nuclear receptor/microRNA circuitry links muscle fiber type to energy metabolism. *J Clin Invest*. 2013;123:2564–2575.

SUPPLEMENTAL MATERIAL

Tables S1-S4 Legends (please see supplemental Excel files):

Table S1. Selected mRNAs transcripts. mRNA transcripts with greater than 2 fold changes and 10% FDR.

Table S2. Co-expression network of the 4,422 genes showing significant variations in response to either sex, or hypertrophy, or the interaction of sex and hypertrophy. Their membership modules are given in the GO and Panther tabs.

Table S3. Genes that showed significant changes in hypertrophy when sex as a co-factor is controlled, significant sex-dependent variation when hypertrophy as a co-factor is controlled, and significant sex-dependent differential hypertrophy-associated changes. Pathway enrichment analysis results are in tab 2.

Table S4. Data set of microRNAs.

Table S5. Overrepresentation of transcription factor (TF) families in identified genes by interaction model

TF Families	Over representation	Z-Score	Gene list for TF family	Full name
V$ZF02	1.7	28.52	Zbtb7a Zbtb7b Zfp148 Zfp202 Zfp219 Zfp281,Zkscan3	zinc finger and BTB domain containing
V$EGRF	1.67	28.03	Egr1 Egr2 Egr3 Egr4, Wt1	early growth response
V$ZF5F	1.96	26.13	Zbtb14	zinc finger and BTB domain containing 14
V$E2FF	1.6	25.97	E2f1 E2f2 E2f3 E2f4 E2f5 E2f6 E2f7 E2f8	E2F transcriptional factor
V$SP1F	1.65	24.15	Sp1 Sp2 Sp3 Sp4 Sp5 Sp6 Sp7 Sp8	trans-acting transcription factor
V$KLFS	1.45	23.15	Klf1 Klf12 Klf13 Klf15 Klf17 Klf2 Klf3 Klf4 Klf6 Klf7 Klf8 Klf9 Klf10 Klf11 Klf16 Klf5	Kruppel-like factor 1 (erythroid)
V$BEDF	1.86	22.62	Zbed4	zinc finger, BED type containing 4provided
V$CTCF	1.68	20.33	Ctcf Ctcfl	
V$PLAG	1.63	19.93	Plag1 Plagl1 Plagl2	
V$MAZF	1.71	19.71	Maz Patz1	
V$GCF2	2.08	19.69	Lrrfip1	
V$NDPK	1.74	18.69	Nme1 Nme2	

Figure S1. qPCR measurement

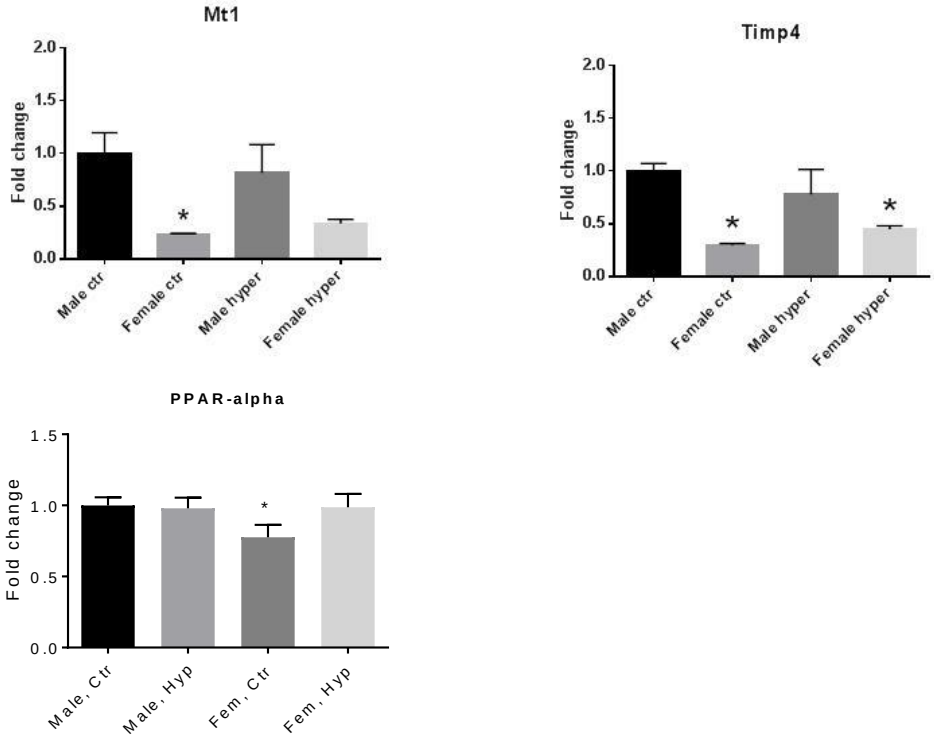

Confirmation of transcripts showing a sex difference. Quantitative polymerace chain reaction (PCR) analysis confirming the RNA-seq data for metallothionein (Mt) and Metalloproteinase inhibitor 4 (TIMP4). mRNA transcripts were quantified using SYBR green (n=3-7 per group). 18s RNA was used for normalizations. Data are mean +/_ standard error measurement (SEM) normalized to the male control. *p<0.05 vs. male control.

Figure S2. Sex differences in expression changes of genes identified by network analysis in figure 7.

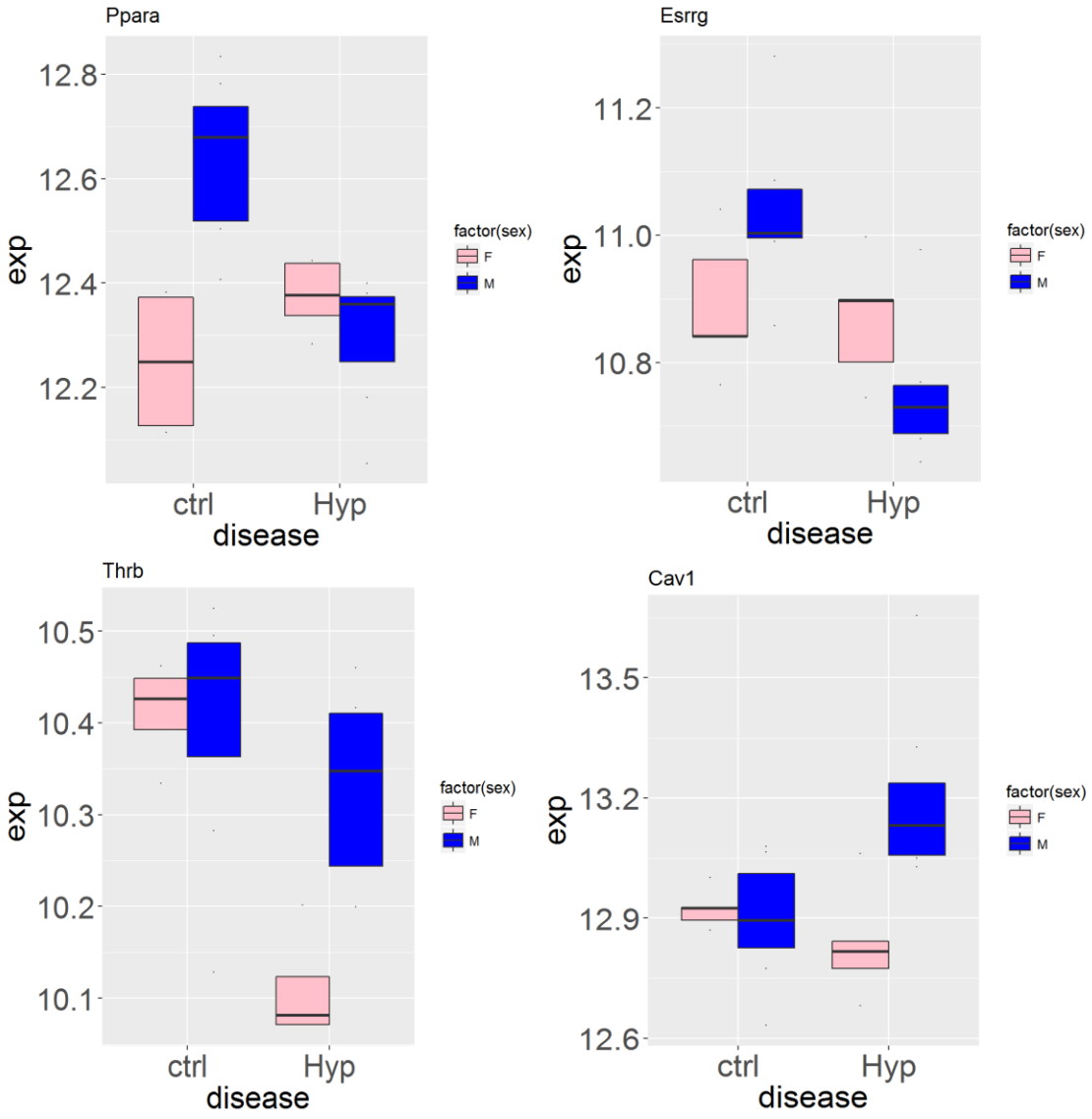

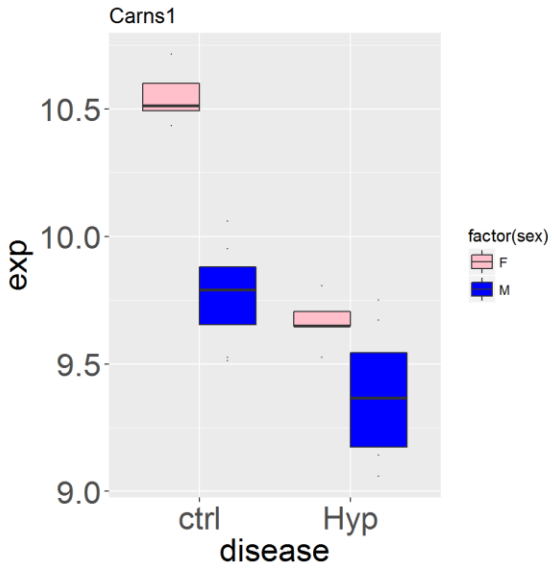
Carns1
10.5
10.0
9.5
9.0
exp
ctrl
Hyp
disease
factor(sex)
F
M

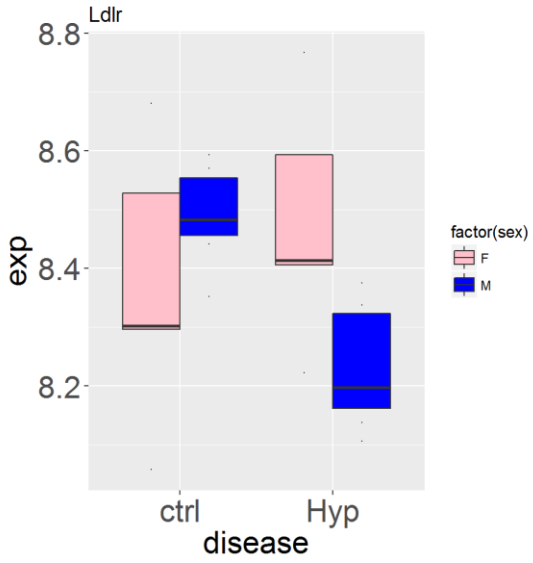
Ldlr
8.8
8.6
8.4
8.2
exp
ctrl
Hyp
disease
factor(sex)
F
M

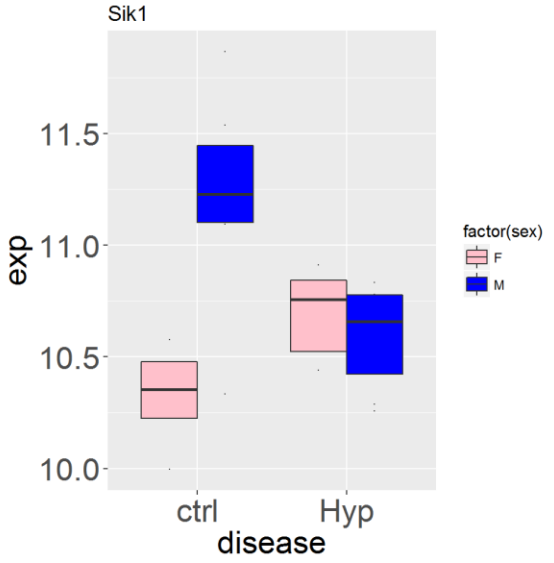
Sik1
11.5
11.0
10.5
10.0
exp
ctrl
Hyp
disease
factor(sex)
F
M

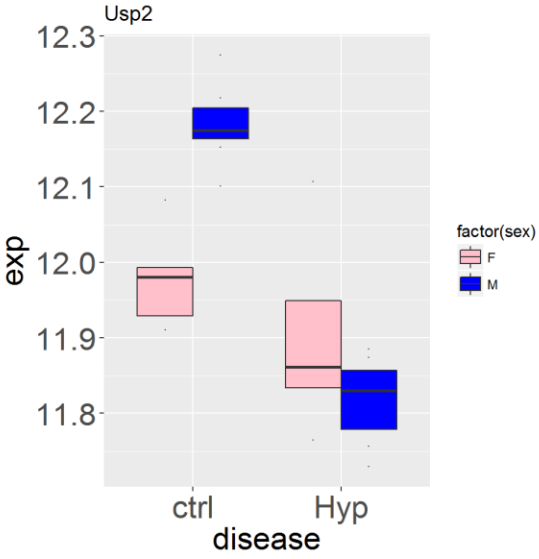
Usp2
12.3
12.2
12.1
12.0
11.9
11.8
exp
ctrl
Hyp
disease
factor(sex)
F
M

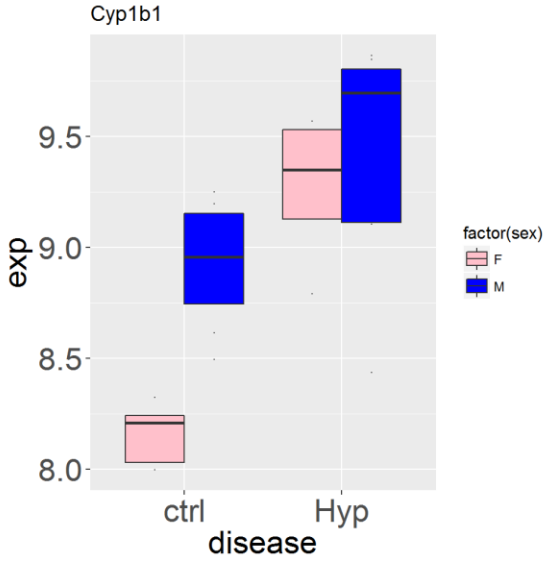
Cyp1b1
9.5
9.0
8.5
8.0
exp
ctrl
Hyp
disease
factor(sex)
F
M

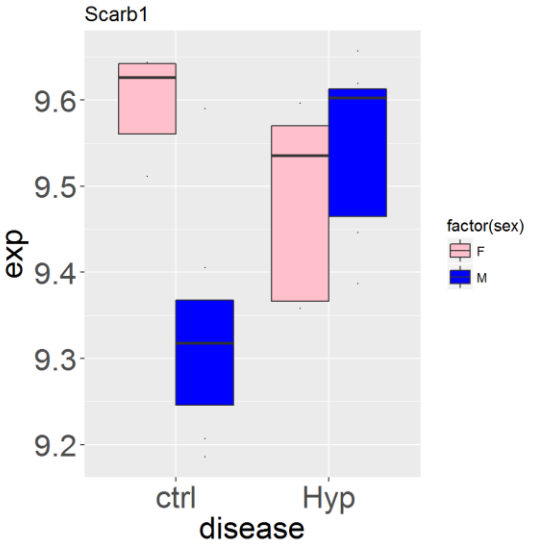
Scarb1
9.6
9.5
9.4
9.3
9.2
exp
ctrl
Hyp
disease
factor(sex)
F
M

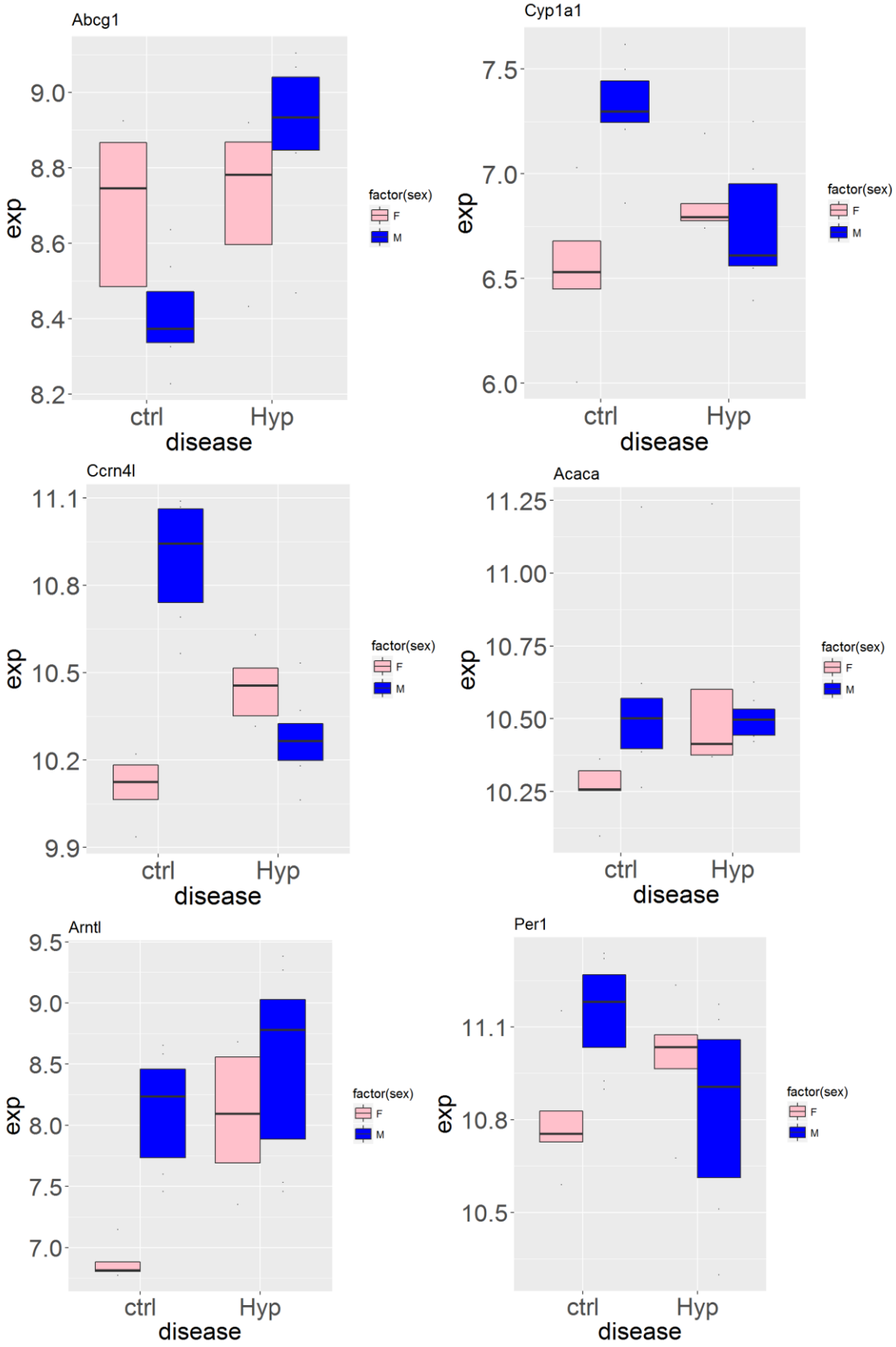
Abcg1
9.0
8.8
8.6
8.4
8.2
exp
ctrl
Hyp
disease
factor(sex)
F
M
Cyp1a1
7.5
7.0
6.5
6.0
exp
ctrl
Hyp
disease
factor(sex)
F
M
Ccrn4l
11.1
10.8
10.5
10.2
9.9
exp
ctrl
Hyp
disease
factor(sex)
F
M
Acaca
11.25
11.00
10.75
10.50
10.25
exp
ctrl
Hyp
disease
factor(sex)
F
M
Arntl
9.5
9.0
8.5
8.0
7.5
7.0
exp
ctrl
Hyp
disease
factor(sex)
F
M
Per1
11.1
10.8
10.5
exp
ctrl
Hyp
disease
factor(sex)
F
M

Figure S3. Volcano plots of miRNA with sex and hypertrophy

A

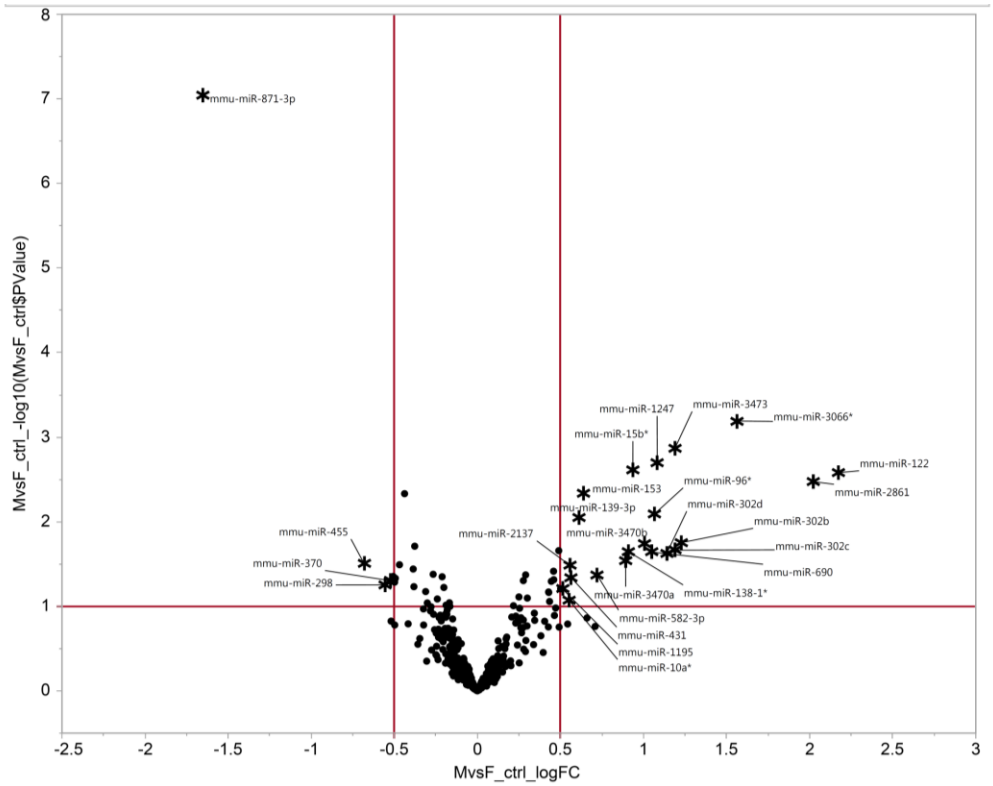

B

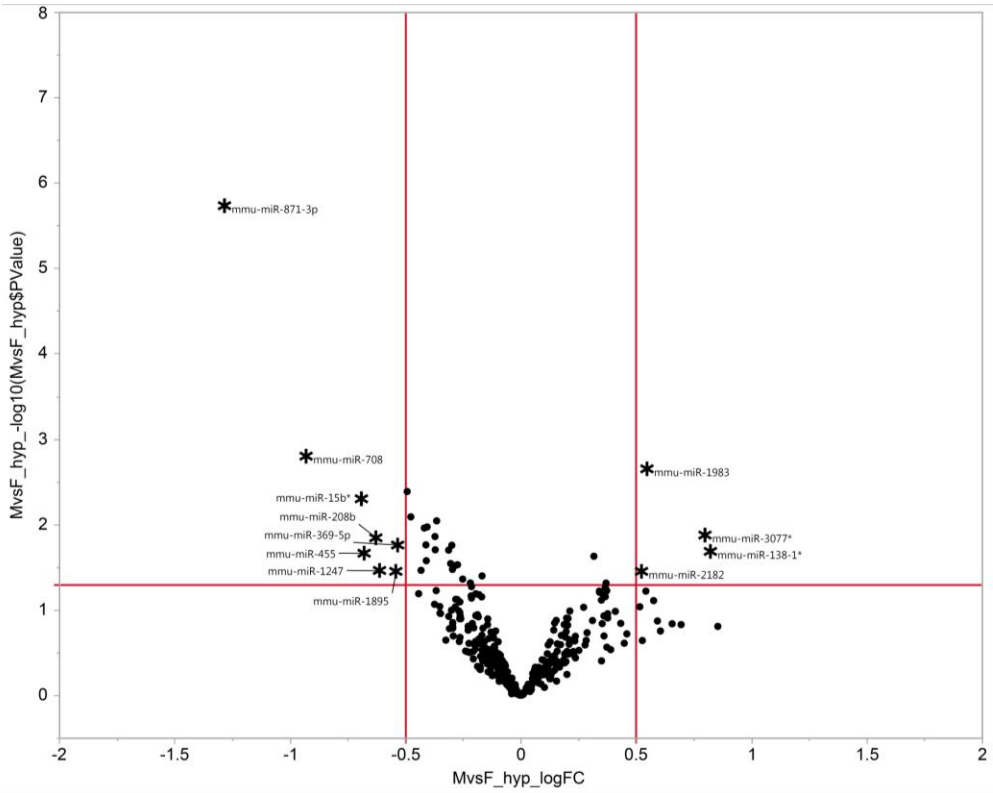

C

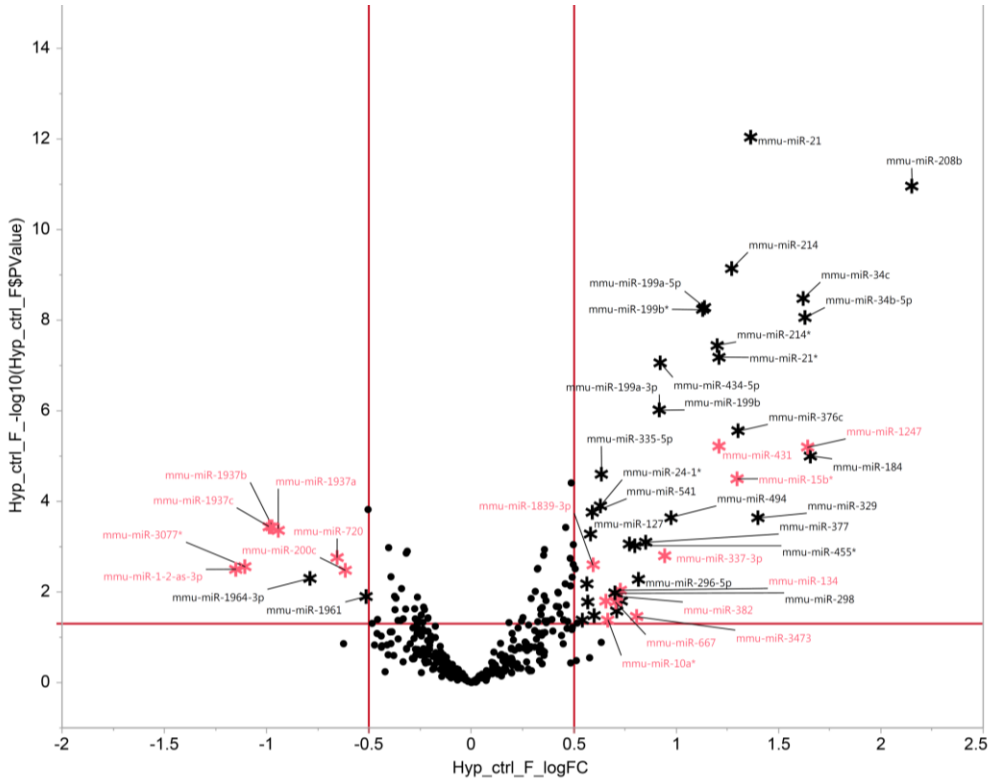
Hyp_ctrl_F_-log10(Hyp_ctrl_F$PValue)
Hyp_ctrl_F_logFC
mmu-miR-21
mmu-miR-208b
mmu-miR-214
mmu-miR-34c
mmu-miR-34b-5p
mmu-miR-199a-5p
mmu-miR-199b*
mmu-miR-214*
mmu-miR-21*
mmu-miR-199a-3p
mmu-miR-434-5p
mmu-miR-199b
mmu-miR-376c
mmu-miR-1247
mmu-miR-335-5p
mmu-miR-431
mmu-miR-184
mmu-miR-1937b
mmu-miR-1937a
mmu-miR-24-1*
mmu-miR-15b*
mmu-miR-1937c
mmu-miR-541
mmu-miR-1839-3p
mmu-miR-494
mmu-miR-329
mmu-miR-127
mmu-miR-377
mmu-miR-3077*
mmu-miR-720
mmu-miR-455*
mmu-miR-200c
mmu-miR-337-3p
mmu-miR-1-2-as-3p
mmu-miR-296-5p
mmu-miR-134
mmu-miR-1964-3p
mmu-miR-298
mmu-miR-1961
mmu-miR-382
mmu-miR-667
mmu-miR-3473
mmu-miR-10a*

D

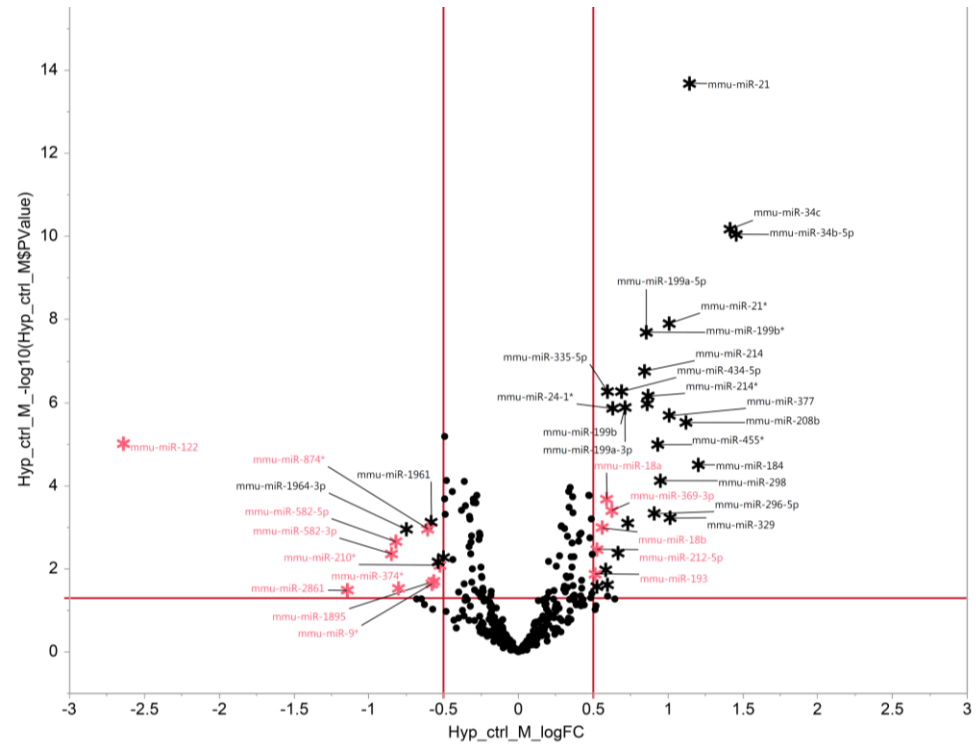
Hyp_ctrl_M_-log10(Hyp_ctrl_M$PValue)
Hyp_ctrl_M_logFC
mmu-miR-21
mmu-miR-34c
mmu-miR-34b-5p
mmu-miR-199a-5p
mmu-miR-21*
mmu-miR-199b*
mmu-miR-335-5p
mmu-miR-214
mmu-miR-434-5p
mmu-miR-24-1*
mmu-miR-214*
mmu-miR-377
mmu-miR-199b
mmu-miR-208b
mmu-miR-199a-3p
mmu-miR-455*
mmu-miR-122
mmu-miR-18a
mmu-miR-184
mmu-miR-874*
mmu-miR-1961
mmu-miR-298
mmu-miR-1964-3p
mmu-miR-369-3p
mmu-miR-582-5p
mmu-miR-296-5p
mmu-miR-582-3p
mmu-miR-329
mmu-miR-18b
mmu-miR-210*
mmu-miR-212-5p
mmu-miR-374*
mmu-miR-193
mmu-miR-2861
mmu-miR-1895
mmu-miR-9*